

## RESEARCH ARTICLE

# Axonal neurofilaments exhibit frequent and complex folding behaviors

J. Daniel Fenn<sup>1,2</sup>  | Paula C. Monsma<sup>1</sup> | Anthony Brown<sup>1</sup> <sup>1</sup>Department of Neuroscience, Ohio State University, Columbus, Ohio, 43210<sup>2</sup>Medical Scientist Training Program, Ohio State University, Columbus, Ohio, 43210**Correspondence**

Anthony Brown, Department of Neuroscience, Ohio State University, Rightmire Hall, 1060 Carmack Road, Columbus, OH 43210.

Email: brown.2302@osu.edu

**Funding information**

NIH Grant Numbers R01 NS038526, S10 OD010383, P30 NS045758, P30 CA016058; NSF Grant Number IOS 1656784

**Abstract**

Neurofilaments are flexible cytoskeletal polymers that are capable of folding and unfolding between their bouts of bidirectional movement along axons. Here we present a detailed characterization of this behavior in cultured neurons using kymograph analysis with approximately 30 ms temporal resolution. We analyzed 781 filaments ranging from 0.6–42  $\mu\text{m}$  in length. We observed complex behaviors including pinch folds, hairpin folds, orientation changes (flips), and occasional severing and annealing events. On average, the filaments spent approximately 40% of their time in some sort of folded configuration. A small proportion of filaments (4%) moved while folded, but most (96%) moved in an outstretched configuration. Collectively, our observations suggest that motors may interact with neurofilaments at multiple points along their length, but preferentially at their ends. In addition, the prevalence of neurofilament folding and the tendency of neurofilaments to straighten out when they move, suggest that an important function of the movement of these polymers in axons may be to maintain them in an outstretched and longitudinally co-aligned configuration. Thus, neurofilament movement may function as much to organize these polymers as to move them, and this could explain why they spend so much time engaged in apparently unproductive bidirectional movement.

**KEYWORDS**

annealing, axonal transport, kymograph, neurofilament, severing

## 1 | INTRODUCTION

Neurofilaments, which are the intermediate filaments of nerve cells, are space-filling cytoskeletal polymers that contribute to the expansion of axon caliber, which is an important determinant of axonal conduction velocity (Hoffman, 1995; Perrot & Eyer, 2013; Waxman, 1980). In large axons they are the most abundant cytoplasmic structure, occupying most of the axonal volume (Friede & Samorajski, 1970; Schnapp & Reese, 1982). In addition to this structural role, neurofilaments are also cargoes of axonal transport that are unique among known intracellular cargoes in that they are non-membranous polymeric structures (Brown, 2014). While there are still many unanswered questions about the mechanism of movement, it is known that the polymers move bidirectionally along microtubule tracks powered by microtubule motors. Their speed is fast on a timeframe of seconds, with average bout velocities of about 1  $\mu\text{m}/\text{s}$  (Fenn, Johnson, Peng, Jung, & Brown, 2018), but slow on a timeframe of hours or days because the rapid

movements are interrupted by prolonged pauses (Brown, 2000; Wang, Ho, Sun, Liem, & Brown, 2000; Brown, Wang, & Jung, 2005).

Neurofilaments are heteropolymers composed of the low (NFL), medium (NFM) and high (NFH) molecular weight neurofilament triplet proteins and internexin, as well as peripherin in peripheral neurons, but their molecular structure is not well understood (Perrot & Eyer, 2013). The subunit proteins all share a central alpha-helical domain called the rod domain that is flanked by largely unstructured amino and carboxy terminal domains of variable length. The rod domains form coiled coil dimers that associate laterally in a staggered antiparallel manner to form tetramer subunits, which in turn associate laterally and longitudinally to form a 10 nm-diameter filament. The long carboxy terminal domains of the neurofilament subunit proteins project outward from the filament backbone giving the filaments an effective diameter of approximately 40–50 nm, thus increasing their space-filling properties (Garcia et al., 2003; Sanchez et al., 2000).

Two notable features of neurofilaments are their length and flexibility. Moving filaments in cultured neurons range from  $<1$  to  $>50$   $\mu\text{m}$  in length, with average lengths of about 5–10  $\mu\text{m}$  (Fenn et al., 2018). An electron microscopic study of bullfrog olfactory nerves calculated the average neurofilament length to be 118  $\mu\text{m}$ , suggesting that neurofilaments can be even longer in vivo (Burton & Wentz, 1992). Neurofilaments are also extremely flexible, with persistence lengths on the order of 100–200 nm (Beck, Deek, Choi et al., 2010). However, despite this flexibility, electron microscopic studies have consistently demonstrated that axonal neurofilaments adopt an extended configuration, aligning longitudinally and in parallel along the long axis of the axon (Hirokawa, 1982; Schnapp & Reese, 1982).

The flexibility of neurofilaments is evident from our observations on these polymers by live-cell imaging. For example, using time-lapse imaging, we previously reported that neurofilaments in axons of cultured neurons frequently scrunch up or fold back on themselves in spite of the slender caliber of those processes (Taylor, Wang, & Brown, 2012). Here we have extended our analysis of neurofilament folding in cultured neurons using streaming acquisition and kymograph analysis with 30 ms temporal resolution. We found that neurofilament folding is even more prevalent than we reported previously, with approximately 40% of the filaments exhibiting folding along at least a portion of their length during the period of observation. We also observed complex and reversible folding behaviors including pinch folds, hairpin folds, and orientation changes (flips), as well as occasional severing and annealing events. When the filaments moved they almost always stretched out into a fully extended state. Intriguingly, however, a small fraction (4%) of the moving filaments moved in a folded configuration. These behaviors offer new insights into the potential mechanisms by which motors interact with and organize neurofilaments in axons.

## 2 | MATERIALS AND METHODS

### 2.1 | Cell culture and transfection

All animal care and use was performed in accordance with federal guidelines and approved by the Ohio State University Institutional Animal Care and Use Committee. Neonatal rat cortical neurons were co-transfected with pEGFP-NFM and pEB3-mCherry cDNA expression constructs by electroporation using an Amaxa Nucleofector (Lonza) set to program O-03 (Fenn et al., 2018) and then cultured at low density with an astrocyte feeder layer using the glial sandwich technique of Banker and colleagues (Kaech & Banker, 2006). The pEGFP-NFM construct encoded an enhanced variant of green fluorescent protein (GFP) linked to the N-terminus of mouse neurofilament protein M (NFM) (Uchida, Alami, & Brown, 2009), and the pEB3-mCherry construct encoded a red fluorescent protein (mCherry) fused to the N-terminus of human microtubule end-binding protein 3 (Efimov et al., 2008). After transfection, the cells were plated onto glass-bottomed culture dishes (assembled using No. 1.5 coverslips) and maintained in NbActiv4<sup>TM</sup> medium (BrainBits). A more detailed description of these procedures is provided in Uchida, Monsma, Fenn, and Brown (2016).

### 2.2 | Live imaging

Live-cell imaging was performed after 7–10 days in vitro using a Nikon TiE inverted epifluorescence microscope equipped with a 100x/1.4NA Plan-Apochromat VC oil immersion objective, a Lumencor SOLA LED light source for epifluorescence illumination, and an Andor iXon Ultra 897 EMCCD camera attached to the microscope side port. The microscope and camera were controlled using MetaMorph software (Molecular Devices). Before imaging, the NbActiv4<sup>TM</sup> medium was replaced with Hibernate-E medium (BrainBits, low fluorescence formulation), which buffers its pH at atmospheric CO<sub>2</sub> concentrations. The temperature on the microscope stage was maintained at 37°C using a Biopetechs objective heater and an Okolab H301-T stage-top incubator with a humidity module. Neurofilaments (EGFP-NFM) were imaged using a Chroma ET-49002 GFP epifluorescence filter cube (Chroma Technology) with the LED light source set to 2.5% of maximum power. Neurofilament movies were acquired in “stream-to-RAM” acquisition mode using 30 ms exposures (plus a 0.3 ms readout time) for 5 or 7.5 min, corresponding to 10,000 or 15,000 frames at 33 frames per second. Microtubule comets (EB3-mCherry) were imaged using a Chroma ET-49008 mCherry epifluorescence filter cube (Chroma Technology) with the LED light source set to 5% of maximum power. Comet movies were acquired in “time-lapse” acquisition mode using 200 ms exposures at 2 s time intervals for a total of 2–5 min.

### 2.3 | Kymograph analysis

Kymographs were generated using Fiji software (Schindelin et al., 2012) and the plugin of Seitz & Surrey (Seitz & Surrey, 2006) with a perpendicular line width of 5 pixels and a maximum value sampling method. The line was drawn manually along the axon with the segmented line tool in Fiji using a maximum projection of the image stack as a guide. The same line was used to generate both the neurofilament and mCherry comet kymographs. Axon orientation was assigned based on the direction of movement of the mCherry comets, which mark the plus ends of growing microtubules (Stepanova et al., 2003; Wang & Brown, 2010). We only analyzed axons that contained at least three visible comets, with at least 95% of the visible comets travelling in the same direction. Movies were excluded from our analysis if axon orientation was ambiguous. A more detailed description of these procedures is provided in Fenn et al. (2018).

Our interpretations of putative folding, severing and annealing events were verified by manual measurement of filament lengths and intensities on linear intensity profiles. The profiles were generated in the horizontal (distance) dimension of the kymographs using the “Plot Profile” feature in Fiji, as well as in select frames of the original raw movies where necessary. Filament length was measured as the end-to-end distance at half height. As far as was possible, we measured the lengths and intensities of the filaments before and after folding, and also in the folded regions during folding, to verify the folded configuration. For example, single and double hairpin folds should result in a 2-fold and 3-fold increase in intensity, respectively, within the folded region.

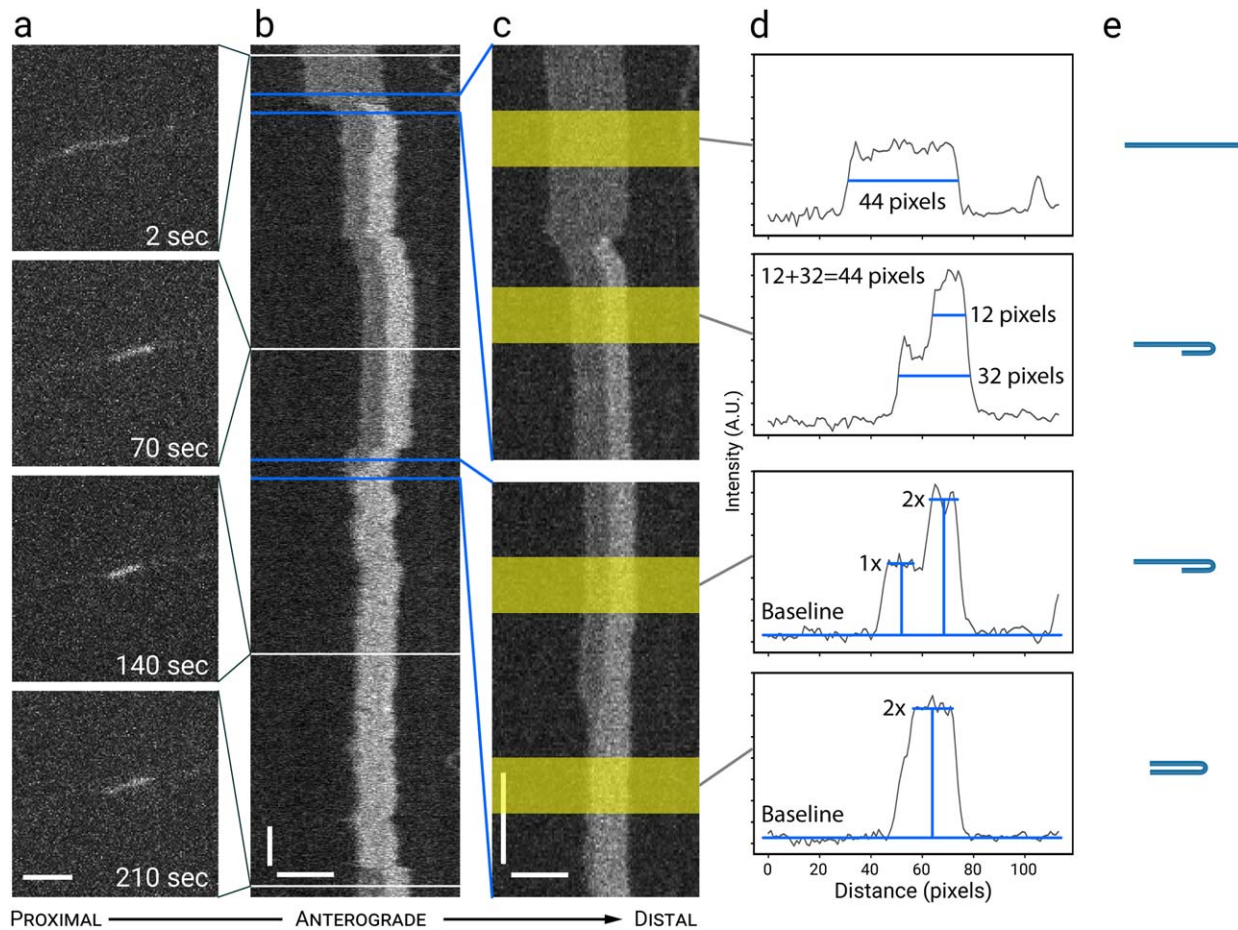


**FIGURE 1** Analysis of neurofilament folding. (a) Raw images from a 10,000-frame movie. Scale bar, 5 μm. (b) A time-compressed kymograph (compressed in the vertical dimension) for the filament shown in (a). The horizontal white lines represent the positions of the raw images in (a). The changes in length and intensity associated with neurofilament folding are hard to discern in the raw images due to the low signal-to-noise ratio, but they are readily apparent in the kymograph due to the spatial alignment of the linear intensity profiles. Horizontal scale bar, 5 μm. Vertical scale bar, 10 s. (c) Two regions of the kymograph in (b), indicated by the blue lines, magnified (i.e. without time compression) to provide higher temporal resolution. In the top panel, the increase in the brightness of the filament at the right (distal) end is accompanied by a decrease in the apparent filament length. In the bottom panel, the filament shortens further to about 50% of its original length, apparently folded in half. Horizontal scale bar, 5 μm. Vertical scale bar, 1 s. (d) Linear intensity profiles from the regions highlighted in yellow in (c). The thickness of the yellow bands (20 pixels) represents the time window that was sampled to generate the average intensity profile. The average intensity is shown in arbitrary units (A.U.). The top two panels show the measurement of filament length. The bottom two panels show the measurement of filament intensity, extending from the baseline to plateau within the folded and unfolded regions. These measurements confirm that the distal end of the filament folded back on itself to create a hairpin fold, with a doubling in the filament intensity in the region of overlap. (e) Schematic of the inferred folding configuration. Note that the filament length is conserved throughout the folding process, consistent with the intensity and length measurements in (d). See Movie S1 in Supporting Information for an excerpt from the raw unprocessed movie upon which this figure is based [Color figure can be viewed at [wileyonlinelibrary.com](http://wileyonlinelibrary.com)]

## 2.4 | Automated edge detection and length measurement

To quantify neurofilament lengths, neurofilament edges were extracted from the kymographs using the Canny-Deriche edge detection algorithm (Deriche, 1987). As we have discussed previously, this algorithm works particularly well for identifying filament edges in our kymographs (Fenn et al., 2018). After Canny-Deriche edge filtering, individual edges were extracted from the kymograph manually using Fiji's auto-wand region selection tool and the coordinates were saved in CSV file format. From this data, filament lengths were recorded for each row of the kymograph. The maximum filament length of each filament was

determined by averaging the highest 0.01% of these length measurements. These steps were automated using the Python 2.7 programming language. Distributions of filament lengths were plotted using the Matplotlib 2.0 package for Python 2.7.

## 2.5 | Electron microscopy

Adult mice (age 20–30 weeks) were anesthetized using CO<sub>2</sub> and sacrificed by cervical dislocation. One leg was shaved quickly and dissected to expose ~2 cm of the tibial nerve in situ, from the knee to the ankle. To ensure that the nerve was fixed at its natural extension, without stretching, twisting or compression, and to avoid handling prior to

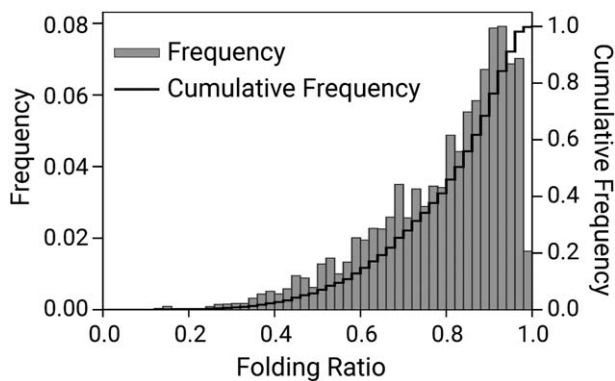


**FIGURE 2** Prevalence and extent of neurofilament folding. For each filament, we calculated the filament length in each timeframe of the kymograph and expressed each of these lengths as a fraction of the maximum filament length for all timeframes for that filament (see Methods). For example, a filament that was folded in half would have a folding ratio of 0.5. Note that this analysis is blind to the configuration of the folded filaments; it simply measures the extent of folding. The folding ratios for all filaments at all time points were then pooled and binned to generate the resulting histogram (bars) and cumulative histogram (stepped line). Note that these are time-weighted distributions in which each filament is represented in proportion to the number of time frames for which it was tracked. Data from 781 filaments across 301 kymographs, representing a total tracking time of 3,775,141 timeframes (~79 hours)

fixation, the entire leg was then removed from the animal, inverted and immersed nerve-down in fixative at room temperature. The time from anesthetization to immersion in fixative was <5 min. The fixative consisted of 2% glutaraldehyde (EM grade, Polysciences, Inc.), 2% formaldehyde (EM grade, Electron Microscopy Sciences), 0.2% tannic acid (low molecular weight, Electron Microscopy Sciences), 0.1 M sodium cacodylate (Polysciences, Inc.), 50 mM sucrose, 0.05% (4.5 mM) calcium chloride (Fisher Scientific), pH 7.4. The tannic acid was dissolved, vortexed vigorously, and added immediately before use. After fixation for 30 min, the nerve was excised, rinsed in a buffer containing 0.1 M sodium cacodylate, 50 mM sucrose and 0.05% (4.5 mM) calcium chloride, pH 7.4, then immersed in 1% osmium tetrachloride (Polysciences, Inc.) in a buffer containing 0.1 M sodium cacodylate and 50 mM sucrose, pH 7.4, for 45 min. The nerve was then rinsed in 3.6% sodium chloride in water and immersed in 5% uranyl acetate (Polysciences, Inc.) in water in the dark for 30 min. After rinsing with water, the nerve was dehydrated through a graded ethanol series (50%, 70%, 80%, 95%, 5 min per rinse), 100% absolute anhydrous ethanol (three rinses, 10 min per rinse), followed by two 10 min rinses in propylene oxide (Polysciences, Inc.). To infiltrate with resin, the nerve was immersed in Poly/Bed 812 resin (Luft's formulation, Polysciences, Inc.) mixed 1:1 with propylene oxide and placed on a rotating mixer for 1 hour, followed by 16–24 hours in resin alone at room temperature. The nerve was cut into segments with a razor blade, then the segments were transferred into fresh resin in silicone embedding molds and polymerized in a vacuum oven at 60°C for 24 hours. Silver sections (~65 nm) were cut using a Diatome diamond knife and Reichert Ultracut E ultramicrotome. Sections were collected on 200-mesh copper grids, stained with uranyl

acetate and lead citrate using standard protocols, and imaged in a FEI Tecnai G2 BioTWIN transmission electron microscope at 80 keV. Images were acquired at microscope magnifications of 14,000 to 39,000 using an AMT Optronix SXR40 digital camera with 1824 × 1824 pixel resolution (Advanced Microscopy Techniques, Woburn, MA).

## 3 | RESULTS

### 3.1 | Kymograph analysis

The observations reported in this paper were derived from a large dataset of movies acquired in a previous study on the kinetic analysis of neurofilament transport (Fenn et al., 2018). Cultured rat cortical neurons co-expressing GFP-tagged neurofilament protein M (GFP-NFM) and microtubule end-binding protein 3 tagged with mCherry (EB3-mCherry) were imaged by epifluorescence microscopy. Single neurofilaments were observed within naturally occurring gaps in the axonal neurofilament array, which arise randomly due to the low neurofilament content of these neurons (Wang & Brown, 2010; Uchida, Colakoglu, Wang, Monsma, & Brown, 2013). Neurofilament movement was recorded by real-time streaming acquisition of the GFP fluorescence with 30.3 ms time resolution. Axon orientation was confirmed by performing time-lapse imaging of EB3-mCherry comets. To analyze the neurofilament and comet movement, we traced a multipoint line segment manually along each axon and generated kymographs along these lines as described in the Methods. In total, we analyzed 781 filaments in 301 kymographs from a total of 136 movies, each lasting for either 10,000 or 15,000 frames (5 min or 7.5 min, respectively).

### 3.2 | The prevalence of folding

Neurofilament folding is manifested in our kymographs as an apparent shortening of the filaments accompanied by an increase in the intensity of the GFP fluorescence along a portion of their length (Taylor et al., 2012) (Figure 1). To quantify the prevalence of folding, we used the Canny-Deriche edge detection algorithm described in Fenn et al. (2018) to locate the edges of the filaments in the kymographs. The x-y coordinates for those edges were then used to calculate the filament length in each 30 ms time interval (i.e. every row of pixels in the kymographs). For each filament, we divided the length at each time interval by the maximum length for that filament, which we considered to be its fully outstretched configuration, and plotted the resulting data as a frequency histogram (Figure 2). The stepped cumulative frequency curve indicates that the filaments spent ~41% of their time folded to  $\leq 80\%$  of their maximal length, ~6% of their time folded to  $\leq 50\%$  of their maximal length, and ~1% of their time folded to  $\leq 33\%$  of their maximal length. Thus, the neurofilaments in these axons are flexible polymers that exhibit frequent and sometimes extensive folding behavior.

### 3.3 | Pinch and hairpin folds

Visual inspection of the kymographs combined with intensity and length measurements as shown in Figure 1 revealed that all folding

events were variations on one of two basic configurations which we term “pinch folds” and “hairpin folds”. Both types of folds were accompanied by a decrease in apparent filament length and a corresponding increase in filament brightness at the site of the fold, and both were reversible. In many cases filaments folded and then straightened out within the period of observation but the duration of each folding event was highly variable, ranging from  $<1$  s to  $>5$  min.

Pinch folds arose as discrete diffraction-limited increases in brightness along the filaments, like a kink along a piece of rope (Figure 3). Such folds were relatively common. Of 781 total filaments analyzed, 78 (10%) exhibited at least one pinch folding event (Table 1). When pinch folds formed near the middle of a filament, both ends tended to pull inward symmetrically (Figure 3a). In contrast, when pinch folds formed near one end of a filament, the ends tended to pull inward asymmetrically, with one end pulling in and the other remaining fixed, as if anchored in some way, or one end pulling in more than the other (Figure 3b–f). Interestingly, when the two ends pulled in asymmetrically there appeared to be no pattern to which end pulled in farther; a pinch near the distal end could result in either the proximal or distal end pulling in farther, and vice versa (compare Figure 3c and f). Filaments also often exhibited more than one pinch folding event during the time of observation, and in one instance we observed two pinch folds at the same time along a single filament, just  $2.9\ \mu\text{m}$  apart (Figure 3d). Interestingly, in four instances we observed a filament with a pinch fold move, and in each case the pinch fold remained fixed in place as if the filament was being pulled through the fold (Figure 3h; Movie S3 in Supporting Information).

Hairpin folds arose when one end of a filament bent back on itself to form a hairpin loop, with a doubling of the fluorescence intensity in the region of overlap of the two strands of the loop (Figure 4). Hairpin folds were the most common folding event, with 114 (15%) of the filaments exhibiting one or more instance (Table 1). It was not unusual for a single filament to exhibit more than one hairpin folding event during the time of observation, and in 15 instances we observed two hairpin folding events at the same time along a single filament. Hairpin folds were observed at both the distal and proximal ends of filaments (compare Figure 4a and d) and the extent of overlap that was created by these folds was variable and often changed gradually or abruptly during the folding event (e.g. Figure 4a). In some cases, the filaments folded completely in half (e.g. Figure 4a and d; Movie S4 in Supporting Information). Interestingly, 31 (27%) of the hairpin folds began as pinch folds that evolved into single or double hairpin folds with a corresponding doubling or tripling of the neurofilament fluorescence intensity in the region of overlap (e.g. Figures 3g and 4c; Movie S2 in Supporting Information).

### 3.4 | Most neurofilaments extend fully when they move

In spite of the widespread and frequent folding behavior described above, the filaments almost always unfurled into a fully extended configuration when they moved. This confirms our previous report

obtained using time-lapse imaging (Taylor et al., 2012). To quantify this, we inspected all the kymographs in our data set visually and scored the appearance of every filament when it moved. We defined movement as a bout in which both ends of the filament moved in parallel in the kymographs, i.e. at comparable velocities, for a distance of at least 10 pixels ( $1.6\ \mu\text{m}$ ). In total, we identified 623 filaments that exhibited one or more bouts of movement, and 598 (96%) of these moved in a fully outstretched (unfolded) configuration. Thus, the folding behaviors described above were largely confined to pauses between bouts of movement, and filaments generally unfolded when they moved (Figure 5). Remarkably, the filaments even remained fully outstretched during repeated reversals. For example, in Figure 5d note that the filament changed direction repeatedly and sometimes abruptly (within 60 ms) without any shortening or increase in brightness along its length (Movie S5 in Supporting Information).

### 3.5 | Though rare, neurofilaments can move while folded

While the vast majority of filaments moved in an unfolded configuration, 25 (4% of all moving filaments) moved while folded (Figure 6). In all cases, the filaments that moved while folded were in a hairpin fold configuration with the apex of the hairpin bend leading, though 3 (12%) of these filaments exhibited short reversals during which the filament moved for short distances with the apex of the hairpin bend trailing (e.g. Figure 10d). Figure 6a shows an example of a filament that moved into the field of view in a hairpin folded configuration and then subsequently unfolded to reveal its full length. Note that this filament was folded in half initially and then unfolded in two stages, first to approximately two-thirds of its true length and then to its full outstretched length. Figure 6b shows a filament that was pausing in a fully extended configuration and then folded in half in a hairpin configuration and moved anterogradely while still folded. Figure 6c shows a pinch fold that originated in the middle of a filament and then extended retrogradely, apparently pulling the entire filament into a hairpin fold and then subsequently moving the filament retrogradely while still in this folded configuration (Movie S6 in Supporting Information).

### 3.6 | Neurofilaments can “flip” their orientation in the axon

Neurofilaments have no structural polarity, but we can detect changes in their orientation by tracking the locations of their proximal and distal ends in the kymographs. For many filaments this was facilitated by the barcoding pattern of the GFP fluorescence which arises due to random incorporation of the GFP-tagged neurofilament protein along the filaments (Fenn et al., 2018). Of the 781 filaments in this study, 184 (24%) exhibited some degree of barcoding. In most cases when a filament folded and unfolded, its proximal-to-distal orientation was preserved. However, 26 (3%) of the filaments in our data set exhibited one or more folding events that led to a switching of their orientation (total of 35 events). We refer to this behavior as flipping. In all flipping events, flipping was generated by a filament end folding back on itself to form

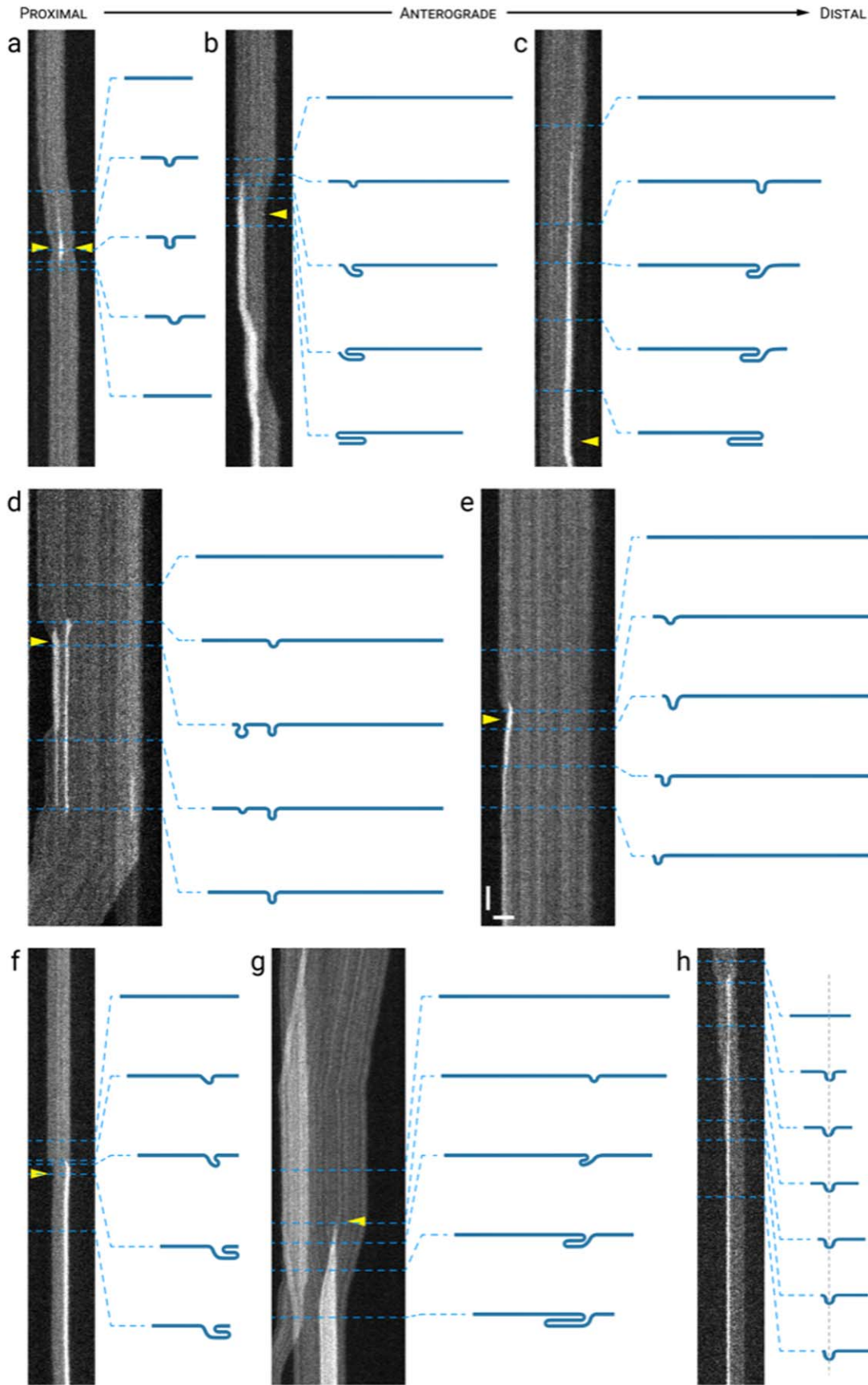


FIGURE 3.

TABLE 1 Data summary

Event	Number of filaments exhibiting event	Total number of events	Percentage of filaments exhibiting event <sup>b</sup>
Hairpin fold	114	203	15%
Pinch fold	78	111	10%
Hairpin and pinch fold	33	33	4%
Flip	26	35	3%
<b>Flip with no reversal</b>			
Pause > Flip > Anterograde	7	7	0.9%
Pause > Flip > Retrograde	4	4	0.5%
Anterograde > Flip > Anterograde	4	4	0.5%
Retrograde > Flip > Retrograde	4	4	0.5%
<b>Flip with reversal</b>			
Anterograde > Flip > Retrograde	3	8	0.4%
Retrograde > Flip > Anterograde	2	8	0.3%
Both <sup>a</sup>	2		0.3%
<b>Movement</b>			
Move outstretched	623		80%
Move folded	598		96% <sup>c</sup>
	25		4% <sup>c</sup>
<b>Annealing</b>			
	10	10	1.3%
<b>Severing</b>			
	7	7	0.9%

A total of 781 filaments in 301 kymographs from 136 movies were scored visually for the occurrence of hairpin folds, pinch folds, flipping events, movement while outstretched events, movement while folded events, end-to-end annealing events, and severing events. A filament was considered to have moved if the midpoint between the filament ends was displaced at least 10 pixels during the course of a single movie. A filament was considered to flip if it changed orientation in the axon so that the end that was proximal was now distal and vice versa. Flipping events were categorized further based on the orientation and directionality of the filament before and after the flipping event. For example, a "Pause > Flip > Anterograde" filament started in a pausing state, flipped orientation, then moved in an anterograde direction. Note that 15% of the filaments exhibited one or more hairpin folding events and 10% of the filaments exhibited one or more pinch folding events, but 4% of the filaments exhibited both pinch and hairpin folding events. Thus 21% of the filaments exhibited one or more folding events overall.

<sup>a</sup>These filaments exhibited one or more bouts of both Anterograde > Flip > Retrograde and Retrograde > Flip > Anterograde reversals.

<sup>b</sup>Percentage of total number of filaments analyzed (781), unless otherwise indicated.

<sup>c</sup>Percentage of total number of filaments that moved (623).

a hairpin bend and then moving towards and past the other end of the filament until the filament unfurled, causing the proximal end to become distal and vice versa. In 24 (69%) of these flipping events, the filament was observed to move both before and after flipping. Intriguingly, in 8 (33%) of these flipping events the direction of movement was retained after the flip (i.e. retrograde-flip-retrograde or

anterograde-flip-antegrade), even though the filament orientation had changed. For these cases the end of the filament that was trailing before the flip became the leading end after the flip, or vice versa. In the remaining 16 (67%) of the cases, the filament reversed direction after the flip (i.e. retrograde-flip-antegrade or anterograde-flip-retrograde). For these cases the end of the filament that was leading before

**FIGURE 3 Pinch folds.** The drawings represent our interpretation of the folding configuration based on measurements of filament length and intensity. The lengths of the filaments in the drawings are drawn to relative scale within each kymograph, but not between kymographs. (a) A transient pinch fold that formed near the center of a filament, appearing to pull both ends of the filament inwards (arrowheads). (b) A pinch fold that formed near the proximal end of a filament and then evolved into what appeared to be a double hairpin fold, appearing to pull the opposite (distal) end inwards (arrowhead) more than the proximal end. (c) A pinch fold that formed near the distal end of a filament and then evolved into what appeared to be a double hairpin fold, appearing to pull the distal end inwards (arrowhead). (d) Two transient pinch folds that formed in close proximity to each other near the proximal end of a filament, appearing to pull the proximal end inwards (arrowhead) in the anterograde direction. The folds subsequently resolved when the proximal end of the filament moved back in the opposite (retrograde) direction. (e) A pinch fold that formed near the proximal end of a filament, appearing to pull the proximal end of the filament inwards (arrowhead) and then translocating toward the proximal end as the filament unfolded. (f) A pinch fold that formed near the distal end of a filament and then evolved into what appeared to be a double hairpin fold, pulling the opposite end of the filament inward. (g) A pinch fold (arrowhead) that formed near the middle of a filament, and then evolved into a double hairpin fold, appearing to pull both the proximal and distal ends of the filament inwards in the process. Note the increase in brightness on the left, which represents overlap of the proximal end of the filament of interest with a shorter filament that paused and then moved away in a retrograde direction. (h) A pinch fold along a moving filament. The pinch fold remained stationary and the filament appeared to "feed through" the pinch as it translocated distally. Horizontal scale bar, 5  $\mu\text{m}$ . Vertical scale bar, 1 s. See Movies S2 and S3 in Supporting Information for animations of the filaments in (g) and (h) [Color figure can be viewed at [wileyonlinelibrary.com](http://wileyonlinelibrary.com)]

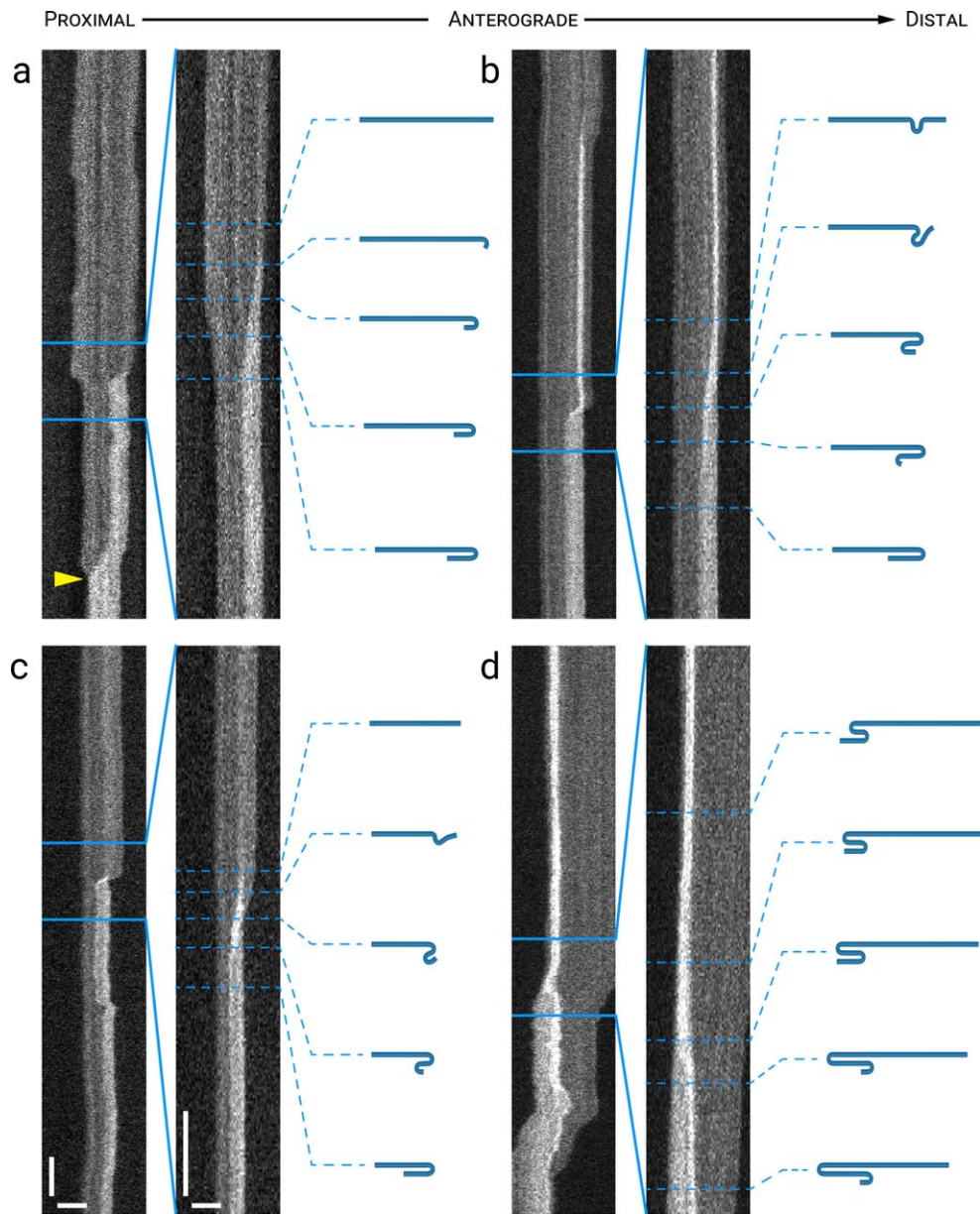


**FIGURE 4** Hairpin folds. Each panel shows a time-compressed kymograph (left) and a portion of that kymograph without time compression (right). The drawings represent our interpretation of the folding configuration based on measurements of filament length and intensity. The lengths of the filaments in the drawings are drawn to relative scale within each kymograph. **(a)** A hairpin fold that formed at the distal end of a filament and progressed until the filament was folded in half (arrowhead). **(b,c)** Evolution of a pinch fold into a double hairpin fold and then subsequently into a single hairpin fold. **(d)** Unfolding of a double hairpin fold close to the proximal end of a filament into a single hairpin fold. Horizontal scale bars, 5  $\mu\text{m}$ . Left vertical scale bar, 5 s. Right vertical scale bar, 1s. See Movie S4 in Supporting Information for an animation of the filament in (a) [Color figure can be viewed at [wileyonlinelibrary.com](http://wileyonlinelibrary.com)]

the flipping event continued to lead, but in the opposite direction, after the flip. There appeared to be no directional preference to this behavior because we observed the same number of retrograde-flip-retrograde events (4) as anterograde-flip-antegrade events (4) and the same number of retrograde-flip-antegrade events (8) as anterograde-flip-retrograde events (8) (Table 1).

Figure 7 shows examples of two flipping events. In Figure 7a, a filament was pausing and fully extended initially, and then its proximal end moved a short distance anterogradely, resulting in a small hairpin fold. That hairpin fold continued moving in an anterograde

direction until the filament flipped end-over-end, reversing its original proximal-distal orientation and then continuing to move anterogradely with what was the proximal end now leading (pause-flip-antegrade; see Movie S7 in Supporting Information). In Figure 7b, a filament entered the field of view traveling in a retrograde direction, flipped end-over-end, and then continued moving in a retrograde direction. Thus, this filament is an example of a flipping event in which the direction of motion was preserved (retrograde-flip-retrograde, in this case) with first one end leading and then the other.

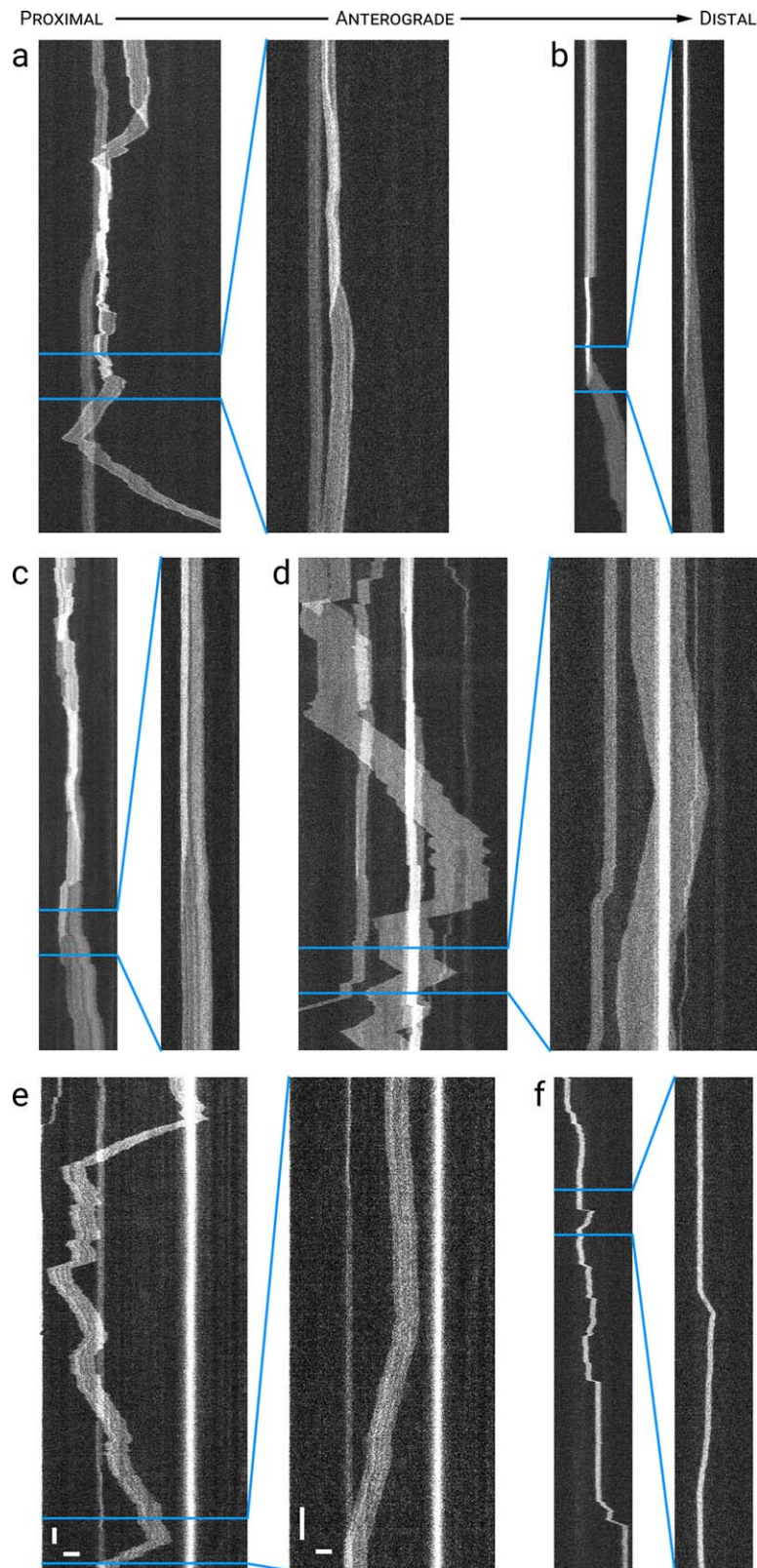


**FIGURE 5** Most filaments unfold when they move. Each panel shows a time-compressed kymograph (left) and a portion of that kymograph without time compression (right). (a-c) Examples of filaments that folded into complex and compact configurations yet stretched out when they moved. (d-f) Examples of filaments that exhibited numerous repeated reversals while remaining outstretched. Note that the filaments often changed direction abruptly (within tens of milliseconds) without folding, as if shuttling backwards and forwards. Horizontal scale bars, 5  $\mu\text{m}$ . Left vertical scale bar, 5 s. Right vertical scale bar, 1 s. See Movie S5 in Supporting Information for an animation of the filament in (d) [Color figure can be viewed at [wileyonlinelibrary.com](http://wileyonlinelibrary.com)]

Figure 8 shows examples of two flipping events that were accompanied by a reversal in the direction of motion. In Figure 8a, a retrogradely moving filament crossed the field of view and then its proximal

end moved anterogradely forming a hairpin fold. Seconds later, the proximal end of this filament continued moving anterogradely, causing the filament to flip end-over-end (retrograde-flip-antegrade; see

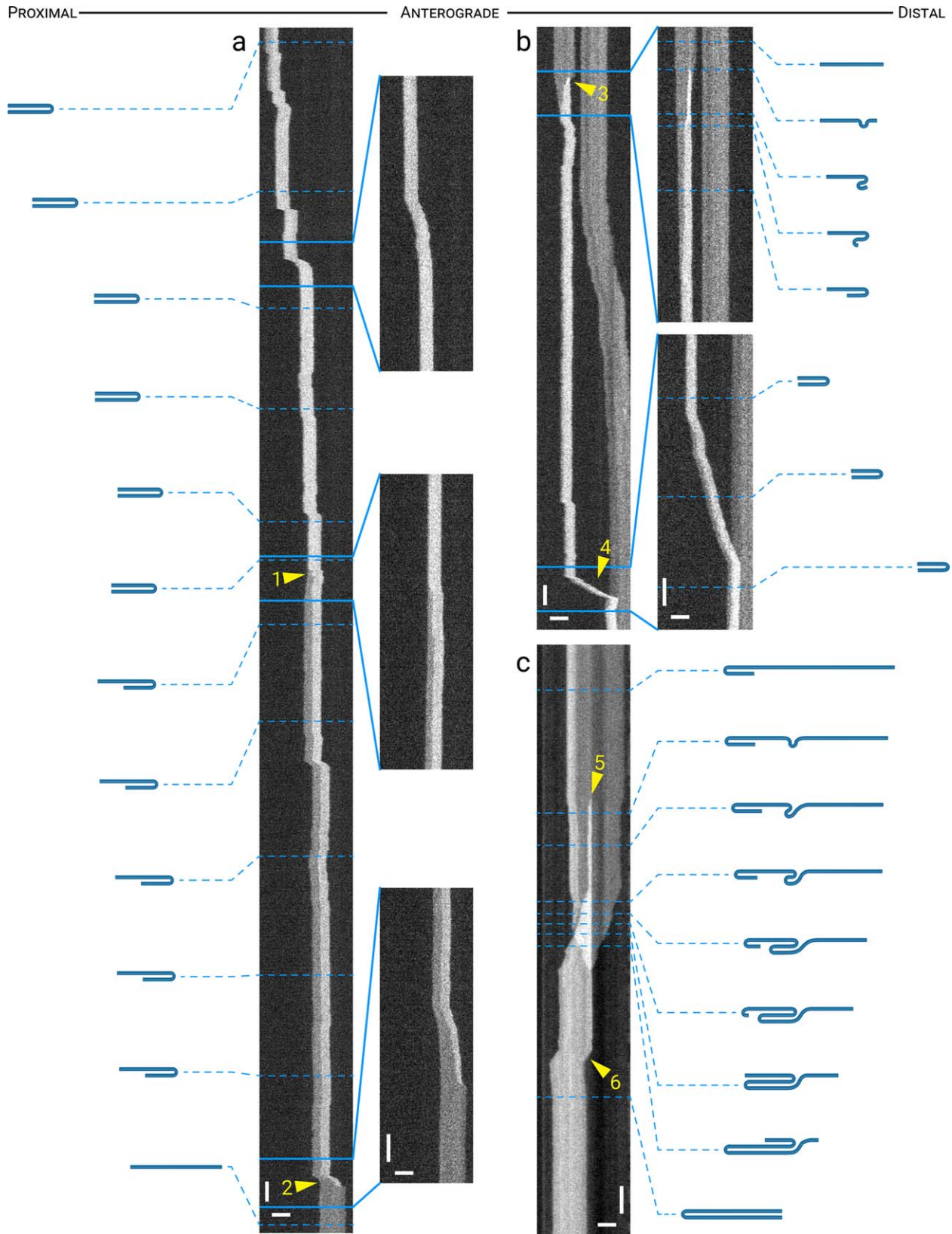


FIGURE 6.

Movie S8 in Supporting Information). In Figure 8b the filament flipped twice, first from retrograde to anterograde and second from anterograde to retrograde. Notably, for this filament the flipping events happened seamlessly with little or no apparent pause prior to the change in the direction of movement.

It is interesting to note that, of the 35 flipping events that we observed, 34 (97%) were accompanied by simultaneous movement of the two filament ends in opposite directions, causing the filament to feed through the hairpin bend as a rope might feed through a pulley or wrap around a pole (Figure 9). We refer to this phenomenon, for want of a better phrase, as “pole wrapping”. For 22 (65%) of these events, the location of the hairpin bend remained fixed, analogous to a fixed pulley (Figure 9a,b,c; Movie S9 in Supporting Information). For the other 12 (35%) “pole-wrapping” events, the location of the hairpin bend drifted in the direction that the leading end of the filament was moving toward, analogous to a drifting pulley (Figure 9d,e,f). If the filaments were completely unconstrained then we would expect flipping to involve one end moving toward and then past the other end, with the latter end remaining fixed in place (until it became the trailing end). The fact that 97% of flipping events involved “pole wrapping” behavior in which both ends moved simultaneously suggests that when neurofilaments fold back on themselves they can glide around other cytoplasmic polymers or organelles that are fully or partially tethered in position.

### 3.7 | Annealing and severing events

We have previously reported that neurofilaments can lengthen by joining ends with other neurofilaments, a process called end-to-end annealing (Çolakoglu & Brown, 2009; Uchida et al., 2013). We have also reported that neurofilaments can be shortened by severing, and we were able to capture annealing and severing events live using time-lapse imaging of cultured neurons (Uchida et al., 2013). To characterize annealing and severing at higher temporal resolution, we searched for these events in our kymographs. To identify annealing events, we looked for instances in which two parent filaments appeared to join ends and then the resulting daughter filament moved as one. To identify severing events, we looked for instances in which the parent filament moved before separating into two daughter filaments so that we could be sure that the parent filament was originally a single filament. In addition

to these criteria, we measured the lengths of the parent and daughter filaments before and after annealing or severing to confirm that filament length was conserved. Of a total of 781 filaments in 301 kymographs (approximately 1,500 min of total tracking time), 10 (1.3%) exhibited an annealing event, corresponding to a frequency of approximately 0.4 annealing events per filament per hour, and 7 (0.9%) exhibited a severing event, corresponding to a frequency of approximately 0.3 severing events per filament per hour. These frequencies are likely to be an underestimate of the actual number of events because we could only confirm severing or annealing if the filaments moved.

Figure 10a,b shows examples of two annealing events. In Figure 10a, a short retrogradely moving neurofilament (1.5  $\mu\text{m}$  in length) crossed the path of a longer anterogradely moving neurofilament (9.0  $\mu\text{m}$  in length) and then the trailing (distal) end of the retrograde filament annealed with the trailing (proximal) end of the anterograde filament and they subsequently moved together in a retrograde direction. In Figure 10b, a short anterogradely moving filament (3.4  $\mu\text{m}$  in length) moved rapidly into the field of view and overlapped with a second short filament (2.4  $\mu\text{m}$  in length) that was pausing. Strikingly, the trailing ends of the two filaments appeared to anneal within one timeframe (30 ms) without any apparent pausing or slowing of the anterogradely moving filament. Collectively, these examples demonstrate that end-to-end annealing of axonal neurofilaments can be remarkably fast.

Figure 10c,d shows examples of two severing events. In Figure 10c the parent filament (20.7  $\mu\text{m}$  in length) moved initially in an anterograde direction, and then paused before separating into two daughter filaments (13.8 and 6.9  $\mu\text{m}$  in length). The more proximal daughter filament remained stationary and the more distal daughter filament moved in a reverse (retrograde) direction, overlapping the other daughter filament. In this example it is intriguing that the severed end of the distal daughter filament became the leading end during its subsequent movement, even though it was originally internal to the parent filament. In addition, it is interesting that the filament intensity brightened in the middle (arrowhead 1) just before the severing event, accompanied by a slight “pulling in” of the proximal (left) end of the filament. It is possible that this represented the time of severing and that the increase in brightness reflects overlap of the daughter filaments. Alternatively, it is also possible the increase in brightness represented a pinch fold and that severing occurred at this site of folding at a later time (arrowhead 2). In

**FIGURE 6 Rare examples of filaments that moved while folded.** Panels (a) and (b) each show a time-compressed kymograph (left) and a portion of that kymograph without time compression (right). Panel (c) shows only an uncompressed kymograph. The drawings represent our interpretation of the folding configuration based on measurements of filament length and intensity. The lengths of the filaments in the drawings are drawn to relative scale within each kymograph, but not between kymographs. **(a)** A filament that entered the kymograph window folded in half in a hairpin configuration and moved rapidly but intermittently in an anterograde direction with the hairpin bend leading before unfurling partially into a two-thirds folded configuration (arrowhead 1). It then continued to move anterogradely with the hairpin bend still leading, but with the bend at a new location along the length of the filament, and then it unfurled completely (arrowhead 2), revealing its length when fully outstretched. Horizontal scale bars, 5  $\mu\text{m}$ . Left vertical scale bar, 5 s. Right vertical scale bar, 1 s. **(b)** An outstretched filament that folded in half in a hairpin configuration (arrowhead 3) while pausing and then moved anterogradely (arrowhead 4) while still folded, with the hairpin bend leading. Horizontal scale bars, 5  $\mu\text{m}$ . Left vertical scale bar, 5 s. Right vertical scale bar, 1 s. **(c)** A pinch fold that formed in the center of a filament (arrowhead 5) and then moved retrogradely, pulling the filament into a hairpin fold. The filament paused briefly and then moved retrogradely again while folded in half (arrowhead 6). Horizontal scale bar, 5  $\mu\text{m}$ . Vertical scale bar, 1 s. See Movie S6 in Supporting Information for an animation of the filament in (c) [Color figure can be viewed at [wileyonlinelibrary.com](http://wileyonlinelibrary.com)]

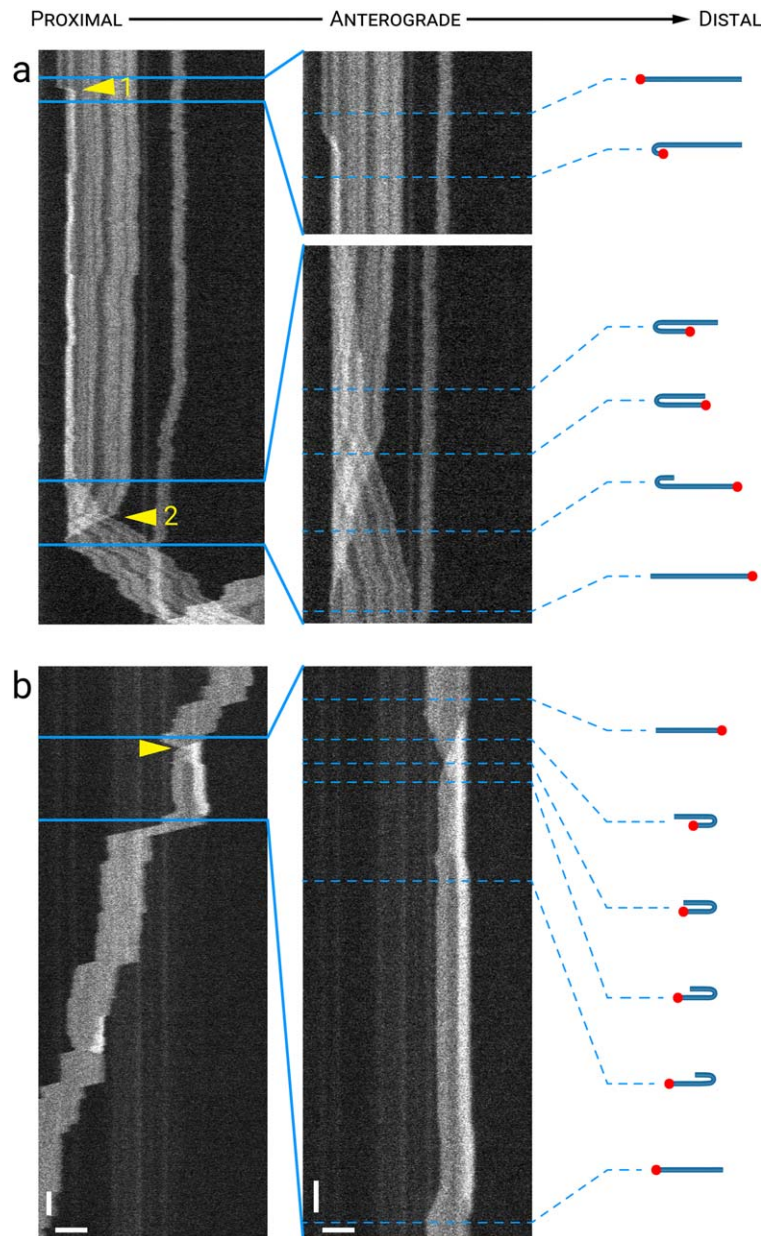


**FIGURE 7** Flipping. Each panel shows a time-compressed kymograph (left) and portions of that kymograph without time compression (right). The drawings represent our interpretation of the folding configuration based on measurements of filament length and intensity. The red dots mark one end of the filament to facilitate tracking it during the flipping event. The lengths of the filaments in the drawings are drawn to relative scale within each kymograph, but not between kymographs. **(a)** A hairpin fold that progressed to a flipping event. The filament was fully extended initially and then formed a hairpin fold at its proximal end (arrowhead 1) about 8 s after the start of the kymograph. Approximately one minute later, this proximal end of the filament resumed movement in the anterograde direction eventually moving past the distal end of the filament (arrowhead 2). As a result, the filament switched orientation within the axon, a fact confirmed by inspection of the barcoding pattern seen along this filament. **(b)** A filament that moved retrogradely, flipped its orientation, and then resumed movement in the same direction with what was the trailing end now leading. The arrowhead indicates the location where the proximal end became the distal end, and vice versa. Horizontal scale bars, 5  $\mu\text{m}$ . Left vertical scale bar, 5 s. Right vertical scale bar, 1 s. See Movie S7 in Supporting Information for an animation of the filament in (a) [Color figure can be viewed at [wileyonlinelibrary.com](http://wileyonlinelibrary.com)]

Figure 10d, the parent filament (8.8  $\mu\text{m}$  in length) moved in an anterograde direction with a hairpin fold at its leading end (quite unusual, but confirmed by measuring the lengths of the filaments before and after severing), and then paused before severing at the apex of the hairpin fold. This resulted in a short filament (2.2  $\mu\text{m}$  in length) that initially

moved retrogradely and then reversed and moved in a net anterograde direction, and a long filament (6.6  $\mu\text{m}$  in length) that paused before also resuming anterograde movement (Movie S10 in Supporting Information). It is tempting to speculate that mechanical strain at the site of the bend may have favored severing at this location.

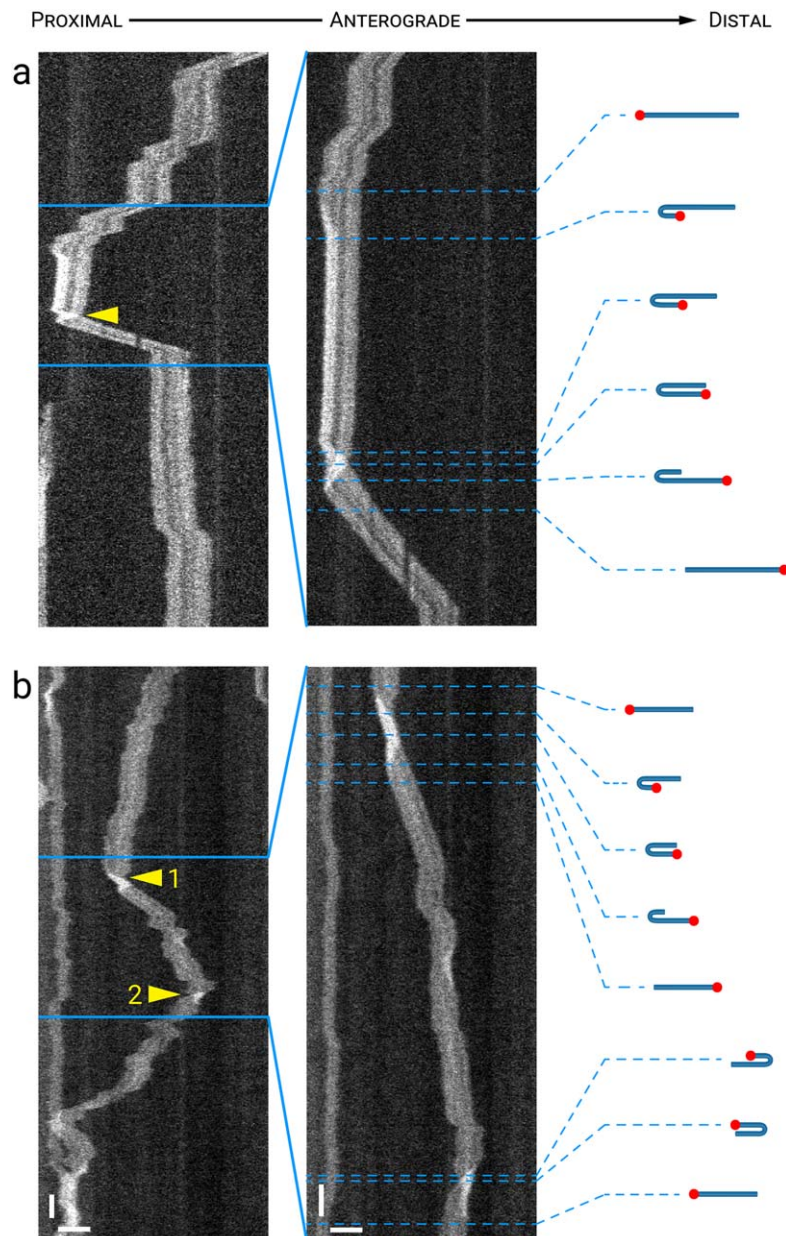


**FIGURE 8** Flipping accompanied by reversals. Each panel shows a time-compressed kymograph (left) and portions of that kymograph without time compression (right). The drawings represent our interpretation of the folding configuration based on measurements of filament length and intensity. The red dots mark one end of the filament to facilitate tracking it during the flipping event. The lengths of the filaments in the drawings are drawn to relative scale within each kymograph, but not between kymographs. **(a)** A filament that moved retrogradely, alternating between bouts of rapid movement and short pauses, then flipped its orientation (arrowhead) and moved anterogradely (retrograde-flip-antegrade). **(b)** A filament that exhibited two flipping events, each associated with a change in the direction of movement; first from retrograde to anterograde (arrowhead 1) and then from anterograde to retrograde (arrowhead 2). Horizontal scale bars, 5  $\mu\text{m}$ . Left vertical scale bar, 5 s. Right vertical scale bar, 1 s. See Movie S8 in Supporting Information for an animation of the filament in (a) [Color figure can be viewed at [wileyonlinelibrary.com](http://wileyonlinelibrary.com)]

### 3.8 | Neurofilament folding in vivo

The prevalence of neurofilament folding described above is surprising because published electron micrographs of neurofilaments in vivo suggest that they are orientated uniformly in a parallel longitudinal array, extending linearly along the long axis of the axon (Schnapp & Reese, 1982; Hirokawa, 1982). Our kymograph analysis relied on the use of cultured neurons with a very low neurofilament

content so that we could identify isolated neurofilaments. However, axons in vivo typically contain hundreds or thousands of neurofilaments in a single axon cross-section, often packed densely with a spacing of  $\sim 30\text{--}60$  nm. Thus, it is reasonable to question whether neurofilament folding is unique to axons in culture with very few neurofilaments, and whether it also occurs in axons in vivo where each filament is typically surrounded by many others. To explore

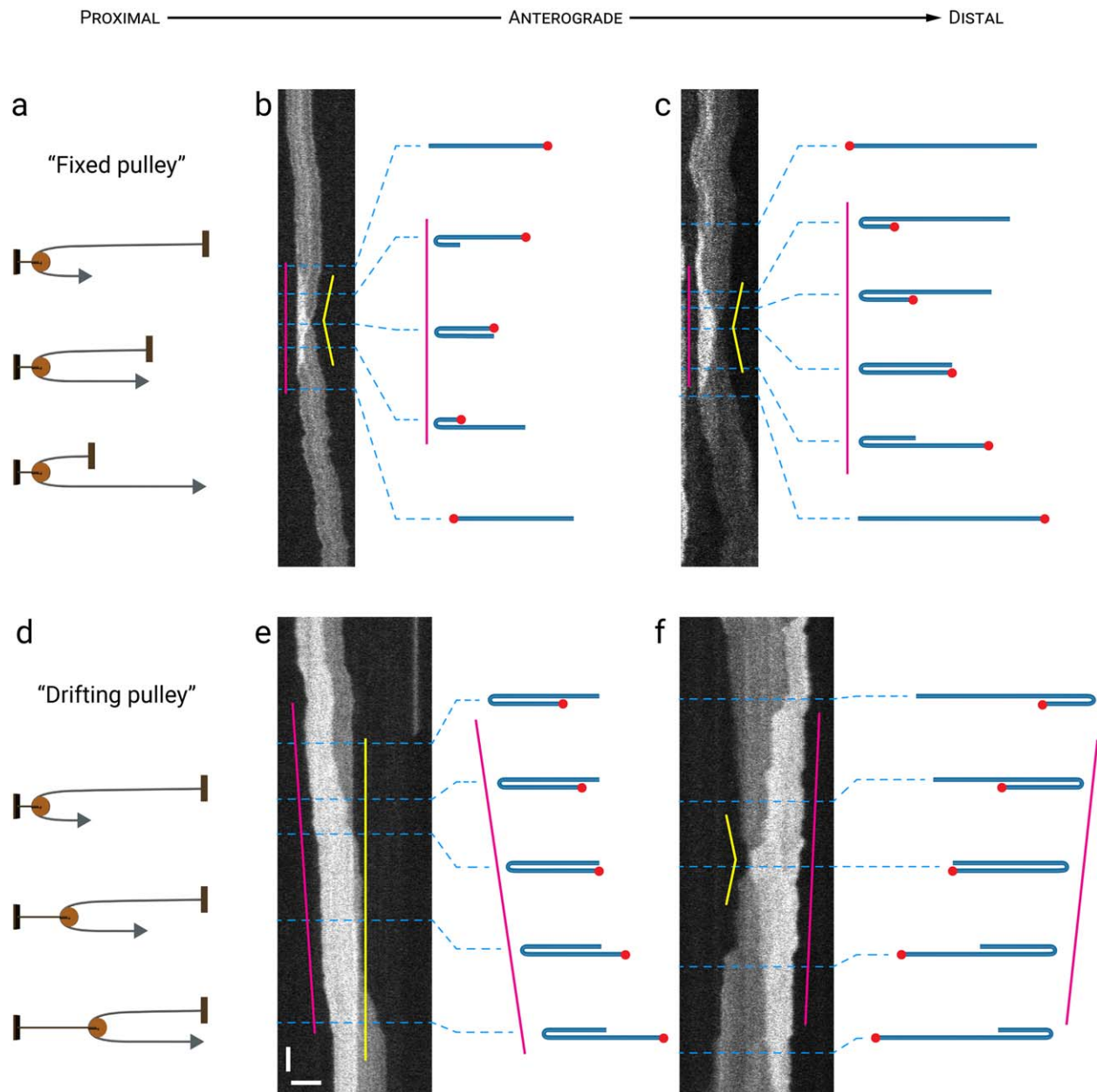


**FIGURE 9** Wrap-around behavior during flipping. Examples of flipping events where the filaments appeared to wrap around an invisible point at the apex of the hairpin fold, like a rope feeding through a pulley. The drawings represent our interpretation of the folding configuration based on measurements of filament length and intensity. The lengths of the filaments in the drawings are drawn to relative scale within each kymograph, but not between kymographs. **(a, b, c)** Schematic and two examples where the apex of the hairpin bend remained fixed (magenta lines) as the filament fed through the bend (“fixed pulley”), causing one end of the filament to move toward the bend as the other moved away (yellow lines). **(d, e, f)** Schematic and two examples where the apex of the hairpin bend drifted (magenta lines) as the filament fed through the bend (“drifting pulley”). In **(e)**, one filament end remained stationary (yellow line) as though tethered, whereas in **(f)** both ends moved (yellow line). Horizontal scale bar, 5  $\mu\text{m}$ . Vertical scale bar, 1 s. See Movie S9 in Supporting Information for an animation of the filament in **(b)** [Color figure can be viewed at [wileyonlinelibrary.com](http://wileyonlinelibrary.com)]

this question, we performed transmission electron microscopy of axons in tibial nerves from adult mice.

Figure 11a-c shows low, medium and high magnification views of four myelinated axons in longitudinal section. Each axon contains hundreds or thousands of neurofilaments aligned roughly parallel to the longitudinal axis of the axon, with microtubules, membranous tubules and organelles interspersed among them. Consistent with

their known flexibility, the neurofilaments are rarely straight, and most often they trace a wavy course. In some regions, the filaments appear to co-align in domains orientated tangential to the long axis. When such domains converge, the filaments appear to intersect in a crisscross pattern giving rise to a meshwork appearance. On close inspection, we also observed many examples of single neurofilaments that curved back on themselves to form a hairpin loop (Figure

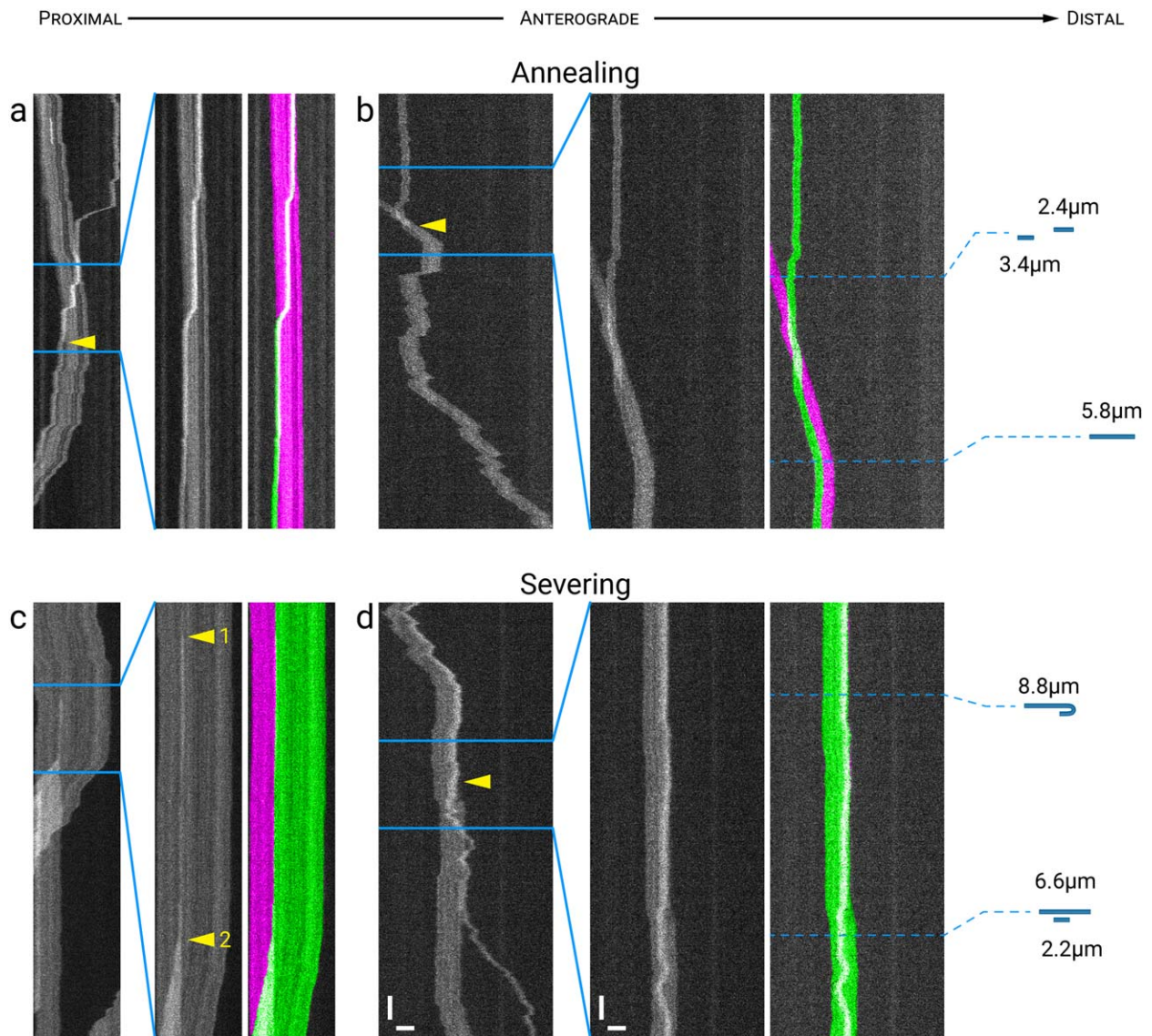


**FIGURE 10 Annealing and severing.** Examples of annealing and severing events. Each panel shows a time-compressed kymograph (left) and portions of that kymograph without time compression (right). The drawings depict the parent and daughter filaments drawn to relative scale. (a) A short retrogradely moving filament crossed paths with a longer anterogradely moving filament and the two then joined together (arrowhead) and moved retrogradely as one filament. The length of the daughter filament ( $10.5\ \mu\text{m}$ ) was equal to the sum of the two parent filaments ( $1.5$  and  $9\ \mu\text{m}$ ). (b) A short anterogradely moving filament crossed paths with a short pausing filament and the two then joined together (arrowhead) and moved anterogradely as one filament. The length of the daughter filament ( $5.8\ \mu\text{m}$ ) was equal to the sum of the two parent filaments ( $2.4$  and  $3.4\ \mu\text{m}$ ). (c) A long filament moved anterogradely, then paused and severed into two daughter filaments. The longer daughter filament then moved retrogradely (opposite to the direction of movement of the parent filament) and passed the shorter daughter filament, which remained paused. The length of the parent filament ( $20.7\ \mu\text{m}$ ) was equal to the sum of the two daughter filaments ( $13.8$  and  $6.9\ \mu\text{m}$ ). The increase in brightness marked by arrowhead 1 was either a pinch fold at the future site of severing, or overlap between the two daughter filaments after severing (see text). Severing is evident when the filaments physically separate (arrowhead 2). (d) A filament with a short hairpin fold at its distal end moved anterogradely, paused, and then severed into two daughter filaments at the apex of the hairpin bend. The arrowhead marks the apparent severing event which appeared to occur at the apex of the hairpin bend. The length of the parent filament ( $8.8\ \mu\text{m}$ ) was equal to the sum of the lengths of the daughter filaments ( $6.6$  and  $2.2\ \mu\text{m}$ ). Horizontal scale bars,  $5\ \mu\text{m}$ . Left vertical scale bar,  $5\ \text{s}$ . Right vertical scale bar,  $1\ \text{s}$ . See Movie S10 in Supporting Information for an animation of the filament in (d) [Color figure can be viewed at [wileyonlinelibrary.com](http://wileyonlinelibrary.com)]

11c-f). Thus, neurofilament organization in these axons is highly polarized but not perfectly ordered, and it is not hard to find examples of filaments that have folded back on themselves. To quantify the frequency and radius of curvature of these looped filaments, we counted and traced all neurofilaments that bent through an arc at

least 2 radians (i.e. twice the radius of curvature) in 23 randomly selected longitudinal axonal profiles (Table 2). The average arc of curvature was 2.7 radians (minimum = 2.0, maximum = 4.0,  $n = 92$ ) and the average radius of curvature was  $65\ \text{nm}$  (minimum =  $23\ \text{nm}$ , maximum =  $174\ \text{nm}$ ,  $n = 92$ ). Note, however, that our electron

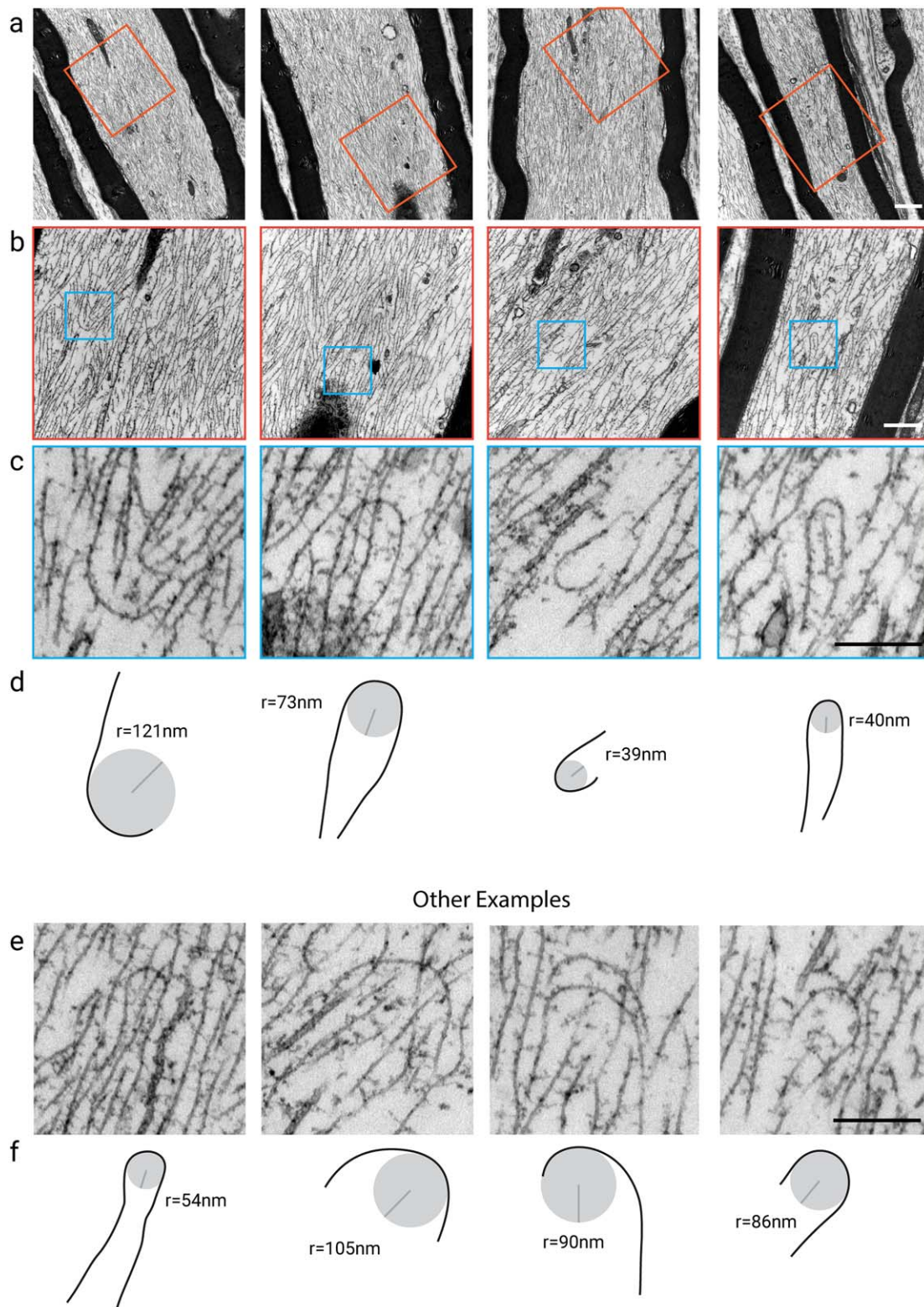


**FIGURE 11** Filament folding in vivo. Transmission electron microscopy of large myelinated axons in the tibial nerve from an adult mouse (longitudinal sections, approximately 65 nm thick). (a) Low magnification views of four different axons. Images acquired at an instrument magnification of 17,000. Scale bar, 1  $\mu\text{m}$ . (b) High magnification views of the regions represented by the orange boxes in (a). Images acquired at an instrument magnification of 39,000. Note that the field of view is rotated due to the helical path of the electron beam. Scale bar, 0.5  $\mu\text{m}$ . (c) Enlarged views of the regions represented by the blue boxes in (b). Scale bar, 0.25  $\mu\text{m}$ . (d) Drawings of the folded filaments in (c), showing their approximate apparent radius of curvature in 2D projection. (e) Four additional examples of folded filaments obtained from other axonal sections. Scale bar, 0.25  $\mu\text{m}$ . (f) Drawings of the folded filaments in (e), showing their approximate apparent radius of curvature in 2D projection (see discussion of caveats in text) [Color figure can be viewed at [wileyonlinelibrary.com](http://wileyonlinelibrary.com)]

TABLE 2 Quantification of curved filaments in vivo

Curved filaments $\geq 2$ radians	Number of filaments	Average	Min	Max
Measured radius of curvature, rad	92	2.7 rad	2 rad	4 rad
Measured radius of curvature, nm		65 nm	23 nm	174 nm
Est. actual radius of curvature, nm		65–92 nm	23–69 nm	174–186 nm
Proportion		0.31%	0	0.67%
Density		$0.16 \mu\text{m}^{-2}$	0	$0.35 \mu\text{m}^{-2}$
Curved filaments $\geq 3$ radians	Number of filaments	Average	Min	Max
Measured radius of curvature, rad	23	3.3 rad	3 rad	4 rad
Measured radius of curvature, nm		57 nm	23 nm	135 nm
Est. actual radius of curvature, nm		57–86 nm	23–69 nm	135–150 nm
Proportion		0.08%	0	0.37%
Density		$0.04 \mu\text{m}^{-2}$	0	$0.19 \mu\text{m}^{-2}$
Total filaments	Total	Average	Min	Max
Density	n/a	$52.4 \mu\text{m}^{-2}$	$36.0 \mu\text{m}^{-2}$	$77.0 \mu\text{m}^{-2}$
Axon area, $\mu\text{m}^2$	$575 \mu\text{m}^2$	$25.0 \mu\text{m}^2$	$10.3 \mu\text{m}^2$	$41.8 \mu\text{m}^2$
Est. total filament number	30,130	1,310	n/a	n/a

We counted and traced all neurofilaments that bent through an arc at least 2 radians (twice the radius of curvature) or 3 radians (three times the radius of curvature, i.e. a hairpin bend) in electron micrographs of 23 randomly selected axons of adult mouse tibial nerve in longitudinal section (23 fields of view in images acquired at a magnification of 14,000–22,500). The statistics shown are the average, minimum and maximum measurements for the 23 fields of view analyzed. Since our electron micrographs represent two-dimensional projections of 65 nm-thick sections, we show the measured radius as well as the estimated range of the actual radius (calculated using the Pythagorean theorem). To estimate the total number of filaments in these micrographs, we counted the number of continuous longitudinal neurofilament profiles in a centrally placed  $1 \mu\text{m}^2$  square region of interest for each axon and then multiplied the resulting average filament density ( $52.4 \mu\text{m}^{-2}$ ) by the total axonal area in those micrographs ( $575 \mu\text{m}^2$ ) to obtain an estimate of the total filament number (30,130). The proportion and density of the filaments that were curved was then calculated by dividing the number of curved filaments counted in those axons by the estimated total filament number or the total axon area, respectively. Most likely these numbers are a significant underestimate because we could only observe hairpin loops if the entire arc of the loop was contained within the 65 nm section.

micrographs represent two-dimensional projections of 65 nm-thick sections, so using the Pythagorean theorem we estimate that the average radius of curvature was in the range 65–92 nm, with a minimum in the range 23–69 nm and a maximum in the range 174–186 nm. This confirms the extraordinary flexibility of these polymers. Twenty-three of the bends in this data set traced an arc of at least 3 radians, i.e. a complete hairpin loop. This corresponds to 0.04 hairpin loops per  $\mu\text{m}^2$  of axonal cytoplasm in longitudinal section. Since the average neurofilament density in these longitudinal sections was 52 neurofilaments per  $\mu\text{m}^2$  (Table 2), this corresponds to approximately 0.1% of the axonal neurofilaments. Most likely this is a significant underestimate because we could only observe hairpin loops if the entire arc of the loop was contained within the 65 nm section. Nevertheless, these data demonstrate that neurofilament folding occurs in vivo and that it is not unique to cultured neurons.

## 4 | DISCUSSION

### 4.1 | Kymograph analysis of neurofilament folding

We previously reported neurofilament folding in axons using time-lapse imaging, but the low temporal resolution of the movies (5 s time intervals) and small sample size (14 folding events) limited our ability to

characterize the folding dynamics (Taylor et al., 2012). In the present study we revisited neurofilament folding using streaming image acquisition at 33 frames per second, which yielded a temporal resolution of approximately 30 ms. We acquired 136 movies (each 10,000 or 15,000 frames in length) of cortical neurons expressing GFP-tagged neurofilaments. From these movies we generated 301 kymographs, permitting us to track 781 neurofilaments and to characterize 314 folding events. The signal-to-noise ratio of the raw movies was low due to the short exposure time, but the spatial alignment of the axial intensity profiles in the kymographs proved to be a very sensitive way to detect changes in length and intensity of the filaments over time. By quantifying those changes, we confirmed that filament lengths and intensities were conserved throughout the folding process.

A potential disadvantage of kymograph analysis for these studies is that it required the generation of linear intensity profiles in each frame of the movie, which resulted in the loss of spatial resolution in the radial dimension of the axon that could potentially aid in the interpretation of the pattern of neurofilament folding. However, in practice this was not a limitation because the axons in our cultures were just a few hundred nanometers in diameter, and therefore diffraction-limited in width, so we were rarely able to resolve the overlapping portions of a filament during a folding event in our movies anyway.

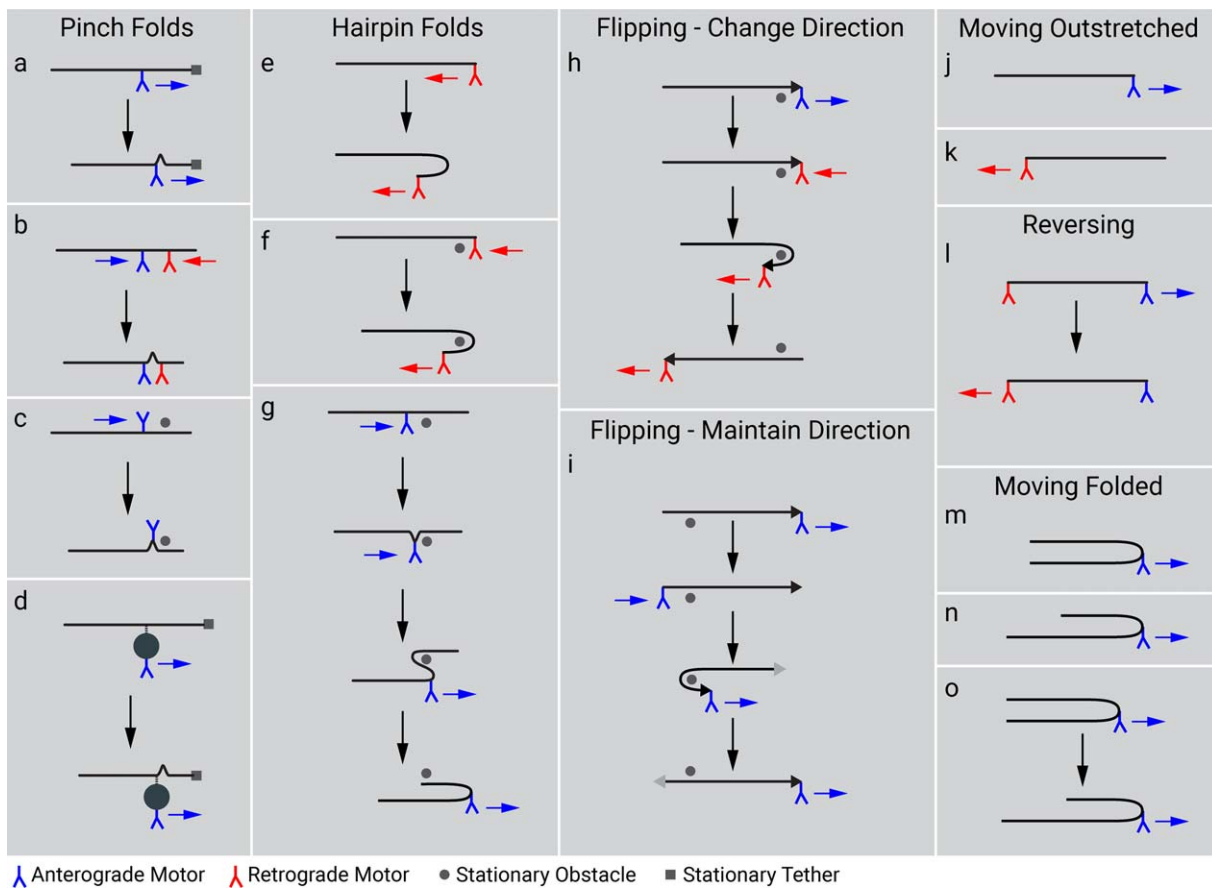


**FIGURE 12 Potential mechanisms of neurofilament folding.** Schematic diagram depicting how forces acting on neurofilaments could explain the diversity of neurofilament folding behaviors. The neurofilaments are represented as horizontal black lines. For the flipping events, one end of the filament is marked with an arrowhead to facilitate tracking of filament orientation. Proximal is left and distal is right throughout. Anterograde and retrograde motors are represented in blue and red, respectively, and the movement of these motors is represented with blue and red arrows. The gray dots represent hypothetical stationary obstacles around which filaments could wrap. The gray squares represent hypothetical stationary objects to which filaments could be tethered. The tethering site is depicted here as being at the distal end of the filament, but it could be at any site along the filament distal to the site of motor attachment. (a) A pinch fold could represent a “buckling” of a filament at the site of motor attachment if one end of the filament is tethered. The tethering site is depicted here as being at the distal end of the filament, but it could be at any site along the filament distal to the site of motor attachment. (b) A pinch fold could also arise if motors of opposing directionality attach to a filament and move towards each other. (c) At least some pinch folds appeared to be generated by a motor pulling the filament from the middle against some obstacle, since pinch folds often evolved into hairpin folds (g). (d) Motors could also act indirectly to generate folding, such as via a membranous organelle that links transiently to a filament as the organelle moves past. (e) Hairpin folds could form if a retrograde motor engaged with the distal end of a filament to form a distal hairpin (shown here) or an anterograde motor engaged with the proximal end to form a proximal hairpin (not shown). (f) In some cases, the apex of the hairpin bend remained fixed in place during the evolution of the hairpin fold, implying that the filament wrapped around some obstacle in the axon. (g) A pinch fold in the interior of a filament could evolve into a double hairpin fold by a motor pulling the filament around an obstacle. (h) Some filaments changed their direction of movement while simultaneously flipping their proximal/distal orientation. In this example a retrograde motor binds to the distal end of an anterogradely moving filament, reversing the orientation and direction of movement of the filament. Note that the leading end of the filament (black arrowhead) remains the same. (i) Flipping also occurred without a change of directionality. In this case, an anterograde motor binds to the trailing end of an anterogradely moving filament and then pulls the trailing end forwards so that what was the leading end (black arrowhead) is now the trailing end (gray arrowhead). (j,k) The majority of filaments moved in a fully outstretched configuration which implies that motors were bound to their leading ends. (l) Given their flexibility, the movement of filaments in a fully outstretched configuration during reversals implies that motors of opposing directionality can engage with opposite ends of the same filament. The speed of these reversals suggests that these motors could be bound simultaneously (as shown here). (m, n, o) The rare movement of filaments in a hairpin configuration indicates that motors can also bind along the length of the filament, not just at the filament ends. The two arms of the hairpin are equal in length if the motor binds in the middle of the filament (m) and unequal in length if it binds closer to one end than the other (n). In some cases, filaments were observed to transition from the former to the latter or vice versa (o). Overall, these folding behaviors suggest that both anterograde and retrograde motors can engage directly or indirectly with neurofilaments at multiple sites all along their length but with a preference for an association with the filament ends [Color figure can be viewed at [wileyonlinelibrary.com](http://wileyonlinelibrary.com)]

## 4.2 | The nature and prevalence of neurofilament folding

Our analysis revealed two classes of folds which we term hairpin and pinch folds. Hairpin folds formed when one end of a filament looped back on itself to form a hairpin bend, resulting in a doubling of the fluorescence intensity in the region of overlap. Pinch folds formed at any location along the filaments and resulted in the filament ends being pulled closer together, while still pointing in opposite directions. In some cases, a pinch fold internal to a filament evolved into a double hairpin fold with a tripling of the filament intensity in the region of overlap.

The large size of our data set permitted us to quantify the prevalence of these neurofilament folding behaviors. Though we have noted folding anecdotally for many years, we were surprised to discover how common it was. Approximately 25% of the filaments exhibited one or more hairpin and/or pinch folding events during the period of observation, and overall the filaments spent an average of 41% of their time folded to 80% or less of their extended length. This indicates that folding is a remarkably frequent event in the axons of cultured neonatal cortical neurons. We have also observed neurofilament folding in cultured sympathetic neurons (unpublished observations).

Our kymograph analysis relied on the observation of isolated neurofilaments within gaps in the axonal neurofilament array. This was necessary because when axonal neurofilaments overlap they are usually too close together to be resolved by conventional light microscopy. To address whether neurofilament folding also occurs *in vivo*, where neurofilaments are often surrounded by many other neurofilaments, we performed electron microscopy of large neurofilament-rich axons in adult mouse tibial nerves. While the majority of neurofilaments were aligned longitudinally, we found that many fields of view also contained one or more examples of filaments that bent and looped back on themselves. Thus, neurofilament folding also occurs in large myelinated axons *in vivo* and is not unique to cultured neurons or to neurons with low neurofilament content. The average radius of curvature was estimated to be in the range 65–92 nm, which is consistent with published reports on the flexibility of neurofilaments *in vitro* (Beck, Deek, Jones, & Safinya, 2010). This explains how neurofilaments can fold back on themselves even within the tight confines of the narrow axons in our cell cultures. The proportion of the filaments that exhibited hairpin (3 radian) bends was much lower than we encountered in our cultures, but this is likely to be a significant underestimate because we could only detect hairpin bends if the entire arc of the bend was contained within the 65 nm section. A more accurate estimate will require 3D reconstruction of neurofilament organization in axons using serial sectioning or tomography.

## 4.3 | The mechanism of neurofilament transport and folding

Several lines of evidence indicate that neurofilaments move along microtubule tracks powered by kinesin-1 and dynein motors. For

example, microtubule disassembly blocks neurofilament movement whereas microfilament disassembly does not (Francis, Roy, Brady, & Black, et al., 2005), and mutations or experimental manipulations that impair kinesin-1 or dynein function impair neurofilament movement (Xia et al., 2003; Uchida et al., 2009; Wang & Brown, 2010). In addition, there is some evidence for interaction of kinesin-1 and dynein motors with neurofilaments, though the interactions have not been well characterized (Prahlaad, Helfand, Langford, Vale, & Goldman, 2000; Shah, Flanagan, Janmey, & Leterrier, 2000; Yabe, Jung, Chan, & Shea, 2000; Helfand, Loomis, Yoon, & Goldman, 2003; Wagner et al., 2004). The number of motors required to move a neurofilament is not known, but given that a single motor can move an organelle as large as a lipid droplet through cytoplasm in *Drosophila* embryos (Shubeita et al., 2008), it seems likely that a single motor is sufficient to move a neurofilament polymer in axons. The discrete and discontinuous nature of the folding events is not consistent with random diffusive motion, so we suggest that the folding mechanism is active, and most likely due to the action of the same motors that transport these filaments.

If the folding behavior of neurofilaments is a consequence of the action of molecular motors on these polymers, then the precise folding configuration can be used to infer the sites of motor attachment. In Figure 12 we present models of motor attachment that could explain the various folding behaviors we have observed in this study, and these are discussed below. At present, we do not know whether the interaction of motors with neurofilaments is direct or indirect. There is precedent for organelles moving by linking to other moving organelles (Salogiannis & Reck-Peterson, 2017), so formally speaking we cannot rule out the possibility that neurofilaments may ride piggyback on another moving cargo such as an organelle. This possible mechanism is depicted for a pinch fold in Figure 12d. However, for simplicity we draw the other motor interactions in Figure 12 as direct interactions.

## 4.4 | Motors may attach preferentially to filament ends

We have noted previously that neurofilaments move preferentially in a fully outstretched state and we proposed that this may indicate that these polymers are pulled from their leading ends (Taylor et al., 2012). In the present study we were able to analyze a much larger number of filaments and this revealed that, while neurofilaments spend a significant proportion of their time folding, 96% of the filaments moved exclusively in a fully outstretched configuration. Given their flexibility, it seems unlikely that neurofilaments could move this way while being pushed from behind. Thus, we speculate that neurofilament motors may bind preferentially (though not exclusively) to the leading ends of moving filaments (e.g. Figure 12j,k) (Taylor et al., 2012).

The idea that motors may form special preferential associations with neurofilament ends is also supported by some of the folding and flipping behaviors that we observed. For example, hairpin folds appeared to arise by one end of a neurofilament moving towards the other end, causing the filament to loop back on itself. In some cases, this movement continued causing the filament to flip orientation so that what was the proximal end became the distal end and vice versa.

It is hard to conceive how such behaviors could arise other than by a pulling force at the leading end of the filament (Figure 12e,f).

#### 4.5 | Motors may attach to both ends of the same filament

Intermediate filaments are distinct from microtubules and microfilaments in that they have no structural polarity (Herrmann & Aebi, 2016). Thus, the two ends of each filament are believed to be structurally identical. Several of the folding behaviors that we observed also suggest that motors can attach to both ends of the same filament. For example, filaments often reversed direction while remaining fully outstretched, as if being pulled in opposite directions, first from one end and then from the other. This suggests that motors of opposite directionality can attach to opposite ends of a filament. In many cases, the reversals occurred almost instantaneously (within two timeframes, i.e. 60 ms), suggesting that the motors may even be attached simultaneously, as if engaged in a tug-of-war (Figure 12l). Further evidence comes from our observations of flipping events. For example, we observed 4 instances in which a filament moving in the anterograde direction flipped its orientation and then continued moving in the anterograde direction, and 4 other instances in which a filament moving in the retrograde direction flipped its orientation and then continued moving in the retrograde direction. These observations suggest that in some cases motors of the same directionality can attach to opposite ends of the same filament. For example, a filament being pulled anterogradely by a kinesin motor at the leading end, can then have another kinesin motor attach to the trailing end, flip end-over-end using that second motor, and then continue moving in the anterograde direction with the second motor now leading (Figure 12i).

#### 4.6 | Motors of opposing directionality may attach to the same end of the filament

In 16 cases, we observed a filament reverse direction after flipping its orientation so that the leading end remained leading, but in the opposite direction. Eight of these were retrogradely moving filaments that flipped orientation and then moved anterogradely, and 8 others were anterogradely moving filaments that flipped orientation and then moved retrogradely. In some cases, we observed filaments that flipped orientation multiple times in quick succession, switching first from retrograde to anterograde and then from anterograde to retrograde and vice versa. In one case we observed a filament flip its orientation and direction of travel 9 times over the course of 5 min. Collectively, these behaviors suggest that both anterograde and retrograde motors may bind to the same end of a filament (Figure 12h). Whether this binding is simultaneous or sequential, with fast switching of bound motors, is unclear.

#### 4.7 | Motors may also attach along the length of filaments

While the behaviors discussed above suggest that there is a preferential association of motors with the ends of the filaments, our

observations suggest that motors can also bind along the length of the filaments. One line of evidence are the pinch folds, in which a local folding event along the length of a filament resulted in one or both ends of the filament pulling inward. Such folds could arise in a number of ways. One possibility is that a motor bound at one site along the filament and pulled on the filament at that point, causing the filament to buckle ahead of the attachment point (Figure 12a). A second possibility is that two motors bound along the length of the filament and moved towards each other (Figure 12b). A third possibility is that pinch folds were generated by the pulling action of a motor bound at the tip of the pinch fold (Figure 12c). Perhaps the most persuasive evidence for this latter possibility were the pinch folds that evolved into a hairpin fold. Figure 6c shows a particularly revealing example in which a pinch fold originated in the middle of a filament and then extended retrogradely toward its proximal end. This movement generated what appeared to be a double hairpin fold that progressed to a simple hairpin fold in which the filament was folded in half. The folded filament then continued to move with the site of the original pinch (now the apex of the hairpin bend) leading. It is hard to explain how this sequence of events could arise other than by attachment of a motor in the center of the filament which was the site of the pinch fold and the apex of the hairpin bend midway between the filament ends (Figure 12g).

Further evidence of motors interacting along the length of filaments, away from their ends, are the 25 filaments that we observed moving in a folded state. Although these filaments represented only 4% of all moving filaments in our study, they establish a proof of principle. All 25 appeared to be folded in a hairpin configuration and moved with the apex of the hairpin leading. Given the flexibility of neurofilaments, it seems unlikely that these folded polymers were pushed by motors attached to the trailing filament ends. More likely, a motor attached to the middle of these filaments and pulled them, dragging filament ends behind (Figure 12m and n). Of particular interest is the filament in Figure 6a which folded in half and moved in this configuration with the apex of the hairpin bend leading, then subsequently unfolded slightly to a two-thirds configuration, whereupon it continued to move with the apex of the hairpin bend still leading. Thus, this filament appeared to exhibit two sites of motor attachment, though we do not know if those motors bound simultaneously or sequentially (Figure 12o).

#### 4.8 | Filaments may wrap around other structures when they fold

It is intriguing that for 97% of flipping events the filament appeared to snake around a point in the axon with both filament ends moving in opposite directions as if the filament was being fed through an invisible pulley. In some cases, the point remained fixed and in others it drifted proximally or distally during the flipping event (compare Figure 9b and e). Perhaps analogous are the 4 instances in which filaments appeared to “feed through” a pinch fold. These “snake around” or “feed through” behaviors suggest that neurofilaments can wrap around other structures in the axon without actually being physically tethered to them (Figure 12f,g,h). These structures could be other neurofilaments or other

cytoskeletal polymers. Alternatively, it is possible that they could be stationary membranous organelles such as mitochondria, endosomes or endoplasmic reticulum.

#### 4.9 | Neurofilament movement may function as much to organize these polymers as to transport them

Axonal transport is generally considered to be a mechanism to deliver cargoes to sites along the axon or to the axon tip (Brown, 2015). However, studies of neurofilament transport in cultured sympathetic and cortical neurons have demonstrated that the filaments spend a significant fraction of their time moving retrogradely, ranging from 17–53% (Wang et al., 2000; Roy et al., 2000; Wang & Brown, 2001; Uchida & Brown, 2004; Uchida et al., 2009; Fenn et al., 2018). Moreover, kymograph analysis of neurofilament transport with high temporal resolution in cultured neurons has also revealed that the filaments frequently reverse direction with little net movement, shuttling forwards and backwards as if engaged in a tug-of-war (Fenn et al., 2018). A single neurofilament may move many hundreds of microns back and forth yet experience a net translocation of only a few microns. Finally, computational modeling of neurofilament transport in vivo suggests that neurofilaments spend approximately 44% of their time moving retrogradely in distal axons of the sciatic nerve (Jung & Brown, 2009). Thus, it is clear that neurons invest a considerable amount of energy into moving neurofilaments backwards as well as forwards, suggesting that neurofilament movement may serve an important function beyond simply that of a neurofilament delivery system.

A striking feature of neurofilament organization in axons is the longitudinal and parallel alignment of these polymers. In electron micrographs, most neurofilaments trace an undulating path roughly parallel to their neighbors and the long axis of the axon, and are spaced apart from each other by a dense brush border of side-arms that project radially from the neurofilament backbone (Schnapp & Reese, 1982; Mukhopadhyay, Kumar, & Hoh, 2004; Laser-Azogui, Kornreich, Malka-Gibor, & Beck, 2015). In large myelinated axons, neurofilaments are the most abundant structure and occupy most of the axonal volume. Axons that lack neurofilaments have reduced caliber, suggesting that these polymers have a space-filling function (Hoffman et al., 1987; Sakaguchi, Okada, Kitamura, & Kawasaki, 1993; Zhu, Couillard-Despres, & Julien, 1997; Hoffman, 1995). Interspersed among the dense array of neurofilaments in axons are clusters of microtubules, which are the tracks for the movement of neurofilaments and other cargoes. Neurofilaments and membranous organelles measuring up to several hundred nanometers in diameter move along these tracks. These cargoes move through this dense neurofilament network apparently unimpeded, with the surrounding neurofilaments parting in the path of the moving cargoes and closing back together behind them, just as water separates at the prow of a ship and coalesces in its wake.

The movement of organelles through the neurofilament array appears to be possible because the neurofilament side-arms function more to space the polymers apart rather than to hold them together (Price, Lasek, & Katz, 1993; Price, Paggi, Lasek, & Katz, 1988), thereby allowing these polymers to be pushed apart readily. In electron

micrographs, the side-arms can give axoplasm the appearance of a cross-linked network (Hirokawa, 1982; Nakagawa, Chen, Zhang, Kanai, & Hirokawa, 1995; Chen, Nakata, Zhang, & Hirokawa, 2000), but in biophysical terms axoplasm may be better described as a nematic liquid crystal hydrogel (Mukhopadhyay et al., 2004; Jones & Safinya, 2008; Safinya et al., 2013). Liquid crystals are a state of matter that can flow like a liquid but that is composed of units with crystalline order. More specifically, nematic liquid crystals are ones in which the units (in this case, neurofilaments) are loosely aligned with their long axes pointing in essentially the same direction (in this case, the long axis of the axon) but are randomly arranged in the longitudinal dimension (i.e. overlapping and not in register). We speculate that this type of organization is critical for allowing neurofilaments to fulfill their structural space-filling role in axons while at the same time providing minimal resistance to the high volume of organelle traffic required for neuronal function.

A key question is how this highly anisotropic organization of predominantly outstretched axonal neurofilaments is established and maintained given the extraordinary flexibility of these polymers evident in our present study. We speculate that it is maintained dynamically by the actions of molecular motors on the polymers pulling them both anterogradely and retrogradely from opposite ends to straighten them out. According to this model, the nematic liquid crystalline organization of the axonal neurofilament array is a dynamic and fluid architecture actively maintained by motors which are acting constantly on these flexible polymers to stretch them out along the longitudinal axis of the axon and counteract their tendency to fold. Thus, neurofilament movement may function as much to organize these polymers as to transport them down the axon, and this could explain why axonal neurofilaments spend so much time engaged in apparently unproductive bidirectional movement.

#### ACKNOWLEDGMENTS

This work was supported by NIH grant R01 NS038526 and NSF grant IOS 1656784. Live-cell imaging was performed in the Neuroscience Imaging Core, made possible by NIH Shared Instrumentation Grant S10 OD010383 and NIH Center Core Grant P30 NS045758. Electron microscopy was performed in the Campus Microscopy and Imaging Facility, supported in part by NIH Center Core Grant P30 CA016058. The authors thank Elizabeth Stone for helpful comments on the manuscript.

#### ORCID

J. Daniel Fenn  <http://orcid.org/0000-0002-4253-6159>

Anthony Brown  <http://orcid.org/0000-0003-2295-2929>

#### REFERENCES

- Beck, R., Deek, J., Jones, J. B., & Safinya, C. R. (2010). Gel-expanded to gel-condensed transition in neurofilament networks revealed by direct force measurements. *Nature Materials*, 9(1), 40–46.
- Beck, R., Deek, J., Choi, M. C., Ikawa, T., Watanabe, O., Frey, E., . . . Safinya, C. R. (2010). Unconventional salt trend from soft to stiff in single neurofilament biopolymers. *Langmuir*, 26(24), 18595–18599.

- Brown, A. (2000). Slow axonal transport: stop and go traffic in the axon. *Nature Reviews. Molecular Cell Biology*, 1(2), 153–156.
- Brown, A. (2014). Slow axonal transport. In: Caplan M, editor. *Reference Module in the Biomedical Sciences*. Elsevier.
- Brown, A. (2015). Axonal transport. In: Pfaff DW and Volkow ND, editors. *Neuroscience in the 21st century: from basic to clinical*. New York: Springer Publishing p. 333–79.
- Brown, A., Wang, L., & Jung, P. (2005). Stochastic simulation of neurofilament transport in axons: the “stop-and-go” hypothesis. *Molecular Biology of the Cell*, 16(9), 4243–4255.
- Burton, P. R., & Wentz, M. A. (1992). Neurofilaments are prominent in bullfrog olfactory axons but are rarely seen in those of the tiger salamander, *Ambystoma tigrinum*. *The Journal of Comparative Neurology*, 317(4), 396–406.
- Chen, J. G., Nakata, T., Zhang, Z. Z., & Hirokawa, N. (2000). The C-terminal tail domain of neurofilament protein-H (NF-H) forms the crossbridges and regulates neurofilament bundle formation. *Journal of Cell Science*, 113(21), 3861–3869.
- Çolakoglu, G., & Brown, A. (2009). Intermediate filaments exchange subunits along their length and elongate by end-to-end annealing. *The Journal of Cell Biology*, 185(5), 769–777.
- Deriche, R. (1987). Using Canny's criteria to derive a recursively implemented optimal edge detector. *International Journal of Computer Vision*, 1(2), 167–187.
- Efimov, A., Schiefermeier, N., Grigoriev, I., Ohi, R., Brown, M. C., Turner, C. E., ... Kaverina, I. (2008). Paxillin-dependent stimulation of microtubule catastrophes at focal adhesion sites. *Journal of Cell Science*, 121(3), 405–204.
- Fenn, J. D., Johnson, C. M., Peng, J., Jung, P., & Brown, A. (2018). Kymograph analysis with high temporal resolution reveals new features of neurofilament transport kinetics. *Cytoskeleton (Hoboken)*, 75(1), 22–41.
- Francis, F., Roy, S., Brady, S. T., & Black, M. M. (2005). Transport of neurofilaments in growing axons requires microtubules but not actin filaments. *Journal of Neuroscience Research*, 79(4), 442–450.
- Friede, R. L., & Samorajski, T. (1970). Axon caliber related to neurofilaments and microtubules in sciatic nerve fibers of rats and mice. *The Anatomical Record*, 167(4), 379–387.
- Garcia, M. L., Lobsiger, C. S., Shah, S. B., Deerinck, T. J., Crum, J., Young, D., ... Cleveland, D.W. (2003). NF-M is an essential target for the myelin-directed “outside-in” signaling cascade that mediates radial axonal growth. *The Journal of Cell Biology*, 163(5), 1011–1020.
- Helfand, B. T., Loomis, P., Yoon, M., & Goldman, R. D. (2003). Rapid transport of neural intermediate filament protein. *Journal of Cell Science*, 116(Pt 11), 2345–2359.
- Herrmann, H., & Aebi, U. (2016). Intermediate Filaments: Structure and Assembly. *Cold Spring Harbor Perspectives in Biology*, 8(11), a018242.
- Hirokawa, N. (1982). Cross-linker system between neurofilaments, microtubules and membranous organelles in frog axons revealed by quick freeze deep etching method. *The Journal of Cell Biology* 94(1), 129–142.
- Hoffman, P. N. (1995). The synthesis, axonal transport, and phosphorylation of neurofilaments determine axonal caliber in myelinated nerve fibers. *The Neuroscientist*, 1(2), 76–83.
- Hoffman, P. N., Cleveland, D. W., Griffin, J. W., Landes, P. W., Cowan, N. J., & Price, D. L. (1987). Neurofilament gene expression: a major determinant of axonal caliber. *Proceedings of the National Academy of Sciences of the United States of America* 84(10), 3472–3476.
- Jones, J. B., & Safinya, C. R. (2008). Interplay between liquid crystalline and isotropic gels in self-assembled neurofilament networks. *Biophysical Journal*, 95(2), 823–835.
- Jung, P., & Brown, A. (2009). Modeling the slowing of neurofilament transport along the mouse sciatic nerve. *Physical Biology*, 6(4), 046002.
- Kaech, S., & Banker, G. (2006). Culturing hippocampal neurons. *Nature Protocols*, 1(5), 2406–2415.
- Laser-Azogui, A., Kornreich, M., Malka-Gibor, E., & Beck, R. (2015). Neurofilament assembly and function during neuronal development. *Current Opinion in Cell Biology*, 32, 92–101.
- Mukhopadhyay, R., Kumar, S., & Hoh, J. H. (2004). Molecular mechanisms for organizing the neuronal cytoskeleton. *Bioessays*, 26(9), 1017–1025.
- Nakagawa, T., Chen, J., Zhang, Z., Kanai, Y., & Hirokawa, N. (1995). Two distinct functions of the carboxyl-terminal tail domain of NF-M upon neurofilament assembly: Cross-bridge formation and longitudinal elongation of filaments. *The Journal of Cell Biology*, 129(2), 411–429.
- Perrot, R., & Eyer, J. (2013). Neurofilaments: properties, functions, and regulation. In: Dermietzel R, editor. *The Cytoskeleton: Imaging, Isolation, and Interaction*. Springer Science+Business Media.
- Prahlad, V., Helfand, B. T., Langford, G. M., Vale, R. D., & Goldman, R. D. (2000). Fast transport of neurofilament protein along microtubules in squid axoplasm. *Journal of Cell Science*, 113(22), 3939–3946.
- Price, R. L., Lasek, R. J., & Katz, M. J. (1993). Neurofilaments assume a less random architecture at nodes and in other regions of axonal compression. *Brain Research*, 607(1–2), 125–133.
- Price, R. L., Paggi, P., Lasek, R. J., & Katz, M. J. (1988). Neurofilaments are spaced randomly in the radial dimension of axons. *Journal of Neurocytology*, 17(1), 55–62.
- Roy, S., Coffee, P., Smith, G., Liem, R. K. H., Brady, S. T., & Black, M. M. (2000). Neurofilaments are transported rapidly but intermittently in axons: implications for slow axonal transport. *The Journal of Neuroscience*, 20(18), 6849–6861.
- Safinya, C. R., Deek, J., Beck, R., Jones, J. B., Leal, C., Ewert, K. K., & Li, Y. (2013). Liquid crystal assemblies in biologically inspired systems. *Liquid Crystals*, 40(12), 1748–1758.
- Sakaguchi, T., Okada, M., Kitamura, T., & Kawasaki, K. (1993). Reduced diameter and conduction velocity of myelinated fibers in the sciatic nerve of a neurofilament-deficient mutant quail. *Neuroscience Letters*, 153(1), 65–68.
- Salogiannis, J., & Reck-Peterson, S. L. (2017). Hitchhiking: A Non-Canonical Mode of Microtubule-Based Transport. *Trends in Cell Biology*, 27(2), 141–150.
- Sanchez, I., Hassinger, L., Sihag, R. K., Cleveland, D. W., Mohan, P., & Nixon, R. A. (2000). Local control of neurofilament accumulation during radial growth of myelinating axons in vivo: Selective role of site-specific phosphorylation. *The Journal of Cell Biology*, 151(5), 1013–1024.
- Schindelin, J., Arganda-Carreras, I., Frise, E., Kaynig, V., Longair, M., Pietzsch, T., ... Schmid, B. (2012). Fiji: an open-source platform for biological-image analysis. *Nature Methods*, 9(7), 676–682.
- Schnapp, B. J., & Reese, T. S. (1982). Cytoplasmic structure in rapid frozen axons. *The Journal of Cell Biology*, 94(3), 667–679.
- Seitz, A., & Surrey, T. (2006). Processive movement of single kinesins on crowded microtubules visualized using quantum dots. *The EMBO Journal*, 25(2), 267–277.
- Shah, J. V., Flanagan, L. A., Janmey, P. A., & Leterrier, J.-F. (2000). Bidirectional translocation of neurofilaments along microtubules mediated in part by dynein/dynactin. *Molecular Biology of the Cell*, 11(10), 3495–3508.

- Shubeita, G. T., Tran, S. L., Xu, J., Vershinin, M., Cermelli, S., Cotton, S. L., ... Gross, S. P. (2008). Consequences of motor copy number on the intracellular transport of kinesin-1-driven lipid droplets. *Cell*, 135(6), 1098–1107.
- Stepanova, T., Slemmer, J., Hoogenraad, C. C., Lansbergen, G., Dortland, B., De Zeeuw, C. I., ... Galjart, N. (2003). Visualization of microtubule growth in cultured neurons via the use of EB3-GFP (end-binding protein 3-green fluorescent protein). *The Journal of Neuroscience*, 23(7), 2655–2664.
- Taylor, N. J., Wang, L., & Brown, A. (2012). Neurofilaments are flexible polymers that often fold and unfold but they move in a fully extended configuration. *Cytoskeleton (Hoboken)*, 69(7), 535–544.
- Uchida, A., & Brown, A. (2004). Arrival, reversal and departure of neurofilaments at the tips of growing axons. *Molecular Biology of the Cell*, 15(9), 4215–4225.
- Uchida, A., Alami, N. H., & Brown, A. (2009). Tight functional coupling of kinesin-1A and dynein motors in the bidirectional transport of neurofilaments. *Molecular Biology of the Cell*, 20(23), 4997–5006.
- Uchida, A., Monsma, P. C., Fenn, J. D., & Brown, A. (2016). Live-cell imaging of neurofilament transport in cultured neurons. *Methods in Cell Biology*, 131, 21–90.
- Uchida, A., Colakoglu, G., Wang, L., Monsma, P. C., & Brown, A. (2013). Severing and end-to-end annealing of neurofilaments in neurons. *Proceedings of the National Academy of Sciences of the United States of America*, 110, E2696–EE705.
- Wagner, O. I., Ascano, J., Tokito, M., Leterrier, J. F., Janmey, P. A., & Holzbaur, E. L. (2004). The interaction of neurofilaments with the microtubule motor cytoplasmic dynein. *Molecular Biology of the Cell*, 15(11), 5092–5100.
- Wang, L., & Brown, A. (2001). Rapid intermittent movement of axonal neurofilaments observed by fluorescence photobleaching. *Molecular Biology of the Cell*, 12(10), 3257–3267.
- Wang, L., & Brown, A. (2010). A hereditary spastic paraplegia mutation in kinesin-1A/KIF5A disrupts neurofilament transport. *Molecular Neurodegeneration*, 5(1), 52.
- Wang, L., Ho, C.-L., Sun, D., Liem, R. K. H., & Brown, A. (2000). Rapid movement of axonal neurofilaments interrupted by prolonged pauses. *Nature Cell Biology*, 2(3), 137–141.
- Waxman, S. G. (1980). Determinants of conduction velocity in myelinated nerve fibers. *Muscle & Nerve*, 3(2), 141–150.
- Xia, C. H., Roberts, E. A., Her, L. S., Liu, X., Williams, D. S., Cleveland, D. W., & Goldstein, L. S. (2003). Abnormal neurofilament transport caused by targeted disruption of neuronal kinesin heavy chain KIF5A. *The Journal of Cell Biology*, 161(1), 55–66.
- Yabe, J. T., Jung, C. W., Chan, W. K. H., & Shea, T. B. (2000). Phospho-dependent association of neurofilament proteins with kinesin in situ. *Cell Motility and the Cytoskeleton*, 45(4), 249–262.
- Zhu, Q., Couillard-Despres, S., & Julien, J.-P. (1997). Delayed maturation of regenerating myelinated axons in mice lacking neurofilaments. *Experimental Neurology*, 148(1), 299–316.

#### SUPPORTING INFORMATION

Additional Supporting Information may be found online in the supporting information tab for this article.

**How to cite this article:** Fenn JD, Monsma PC, Brown A. Axonal neurofilaments exhibit frequent and complex folding behaviors. *Cytoskeleton*. 2018;75:258–280. <https://doi.org/10.1002/cm.21448>